Supplementary Figures

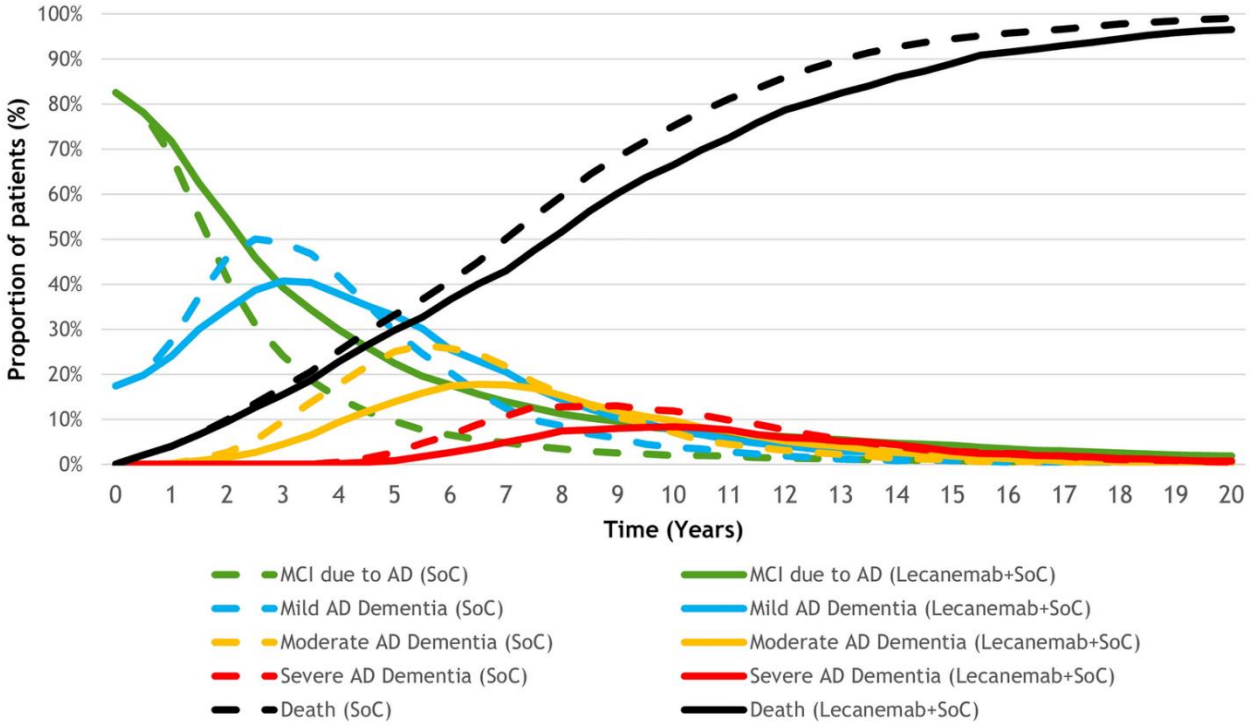

Figure S1. Simulated patient disposition in different AD severity levels or death over lifetime lecanemab compared to standard of care. Abbreviations: AD, Alzheimer's disease; MCI, mild cognitive impairment; SoC, standard of care. Reproduced under open access from [1].

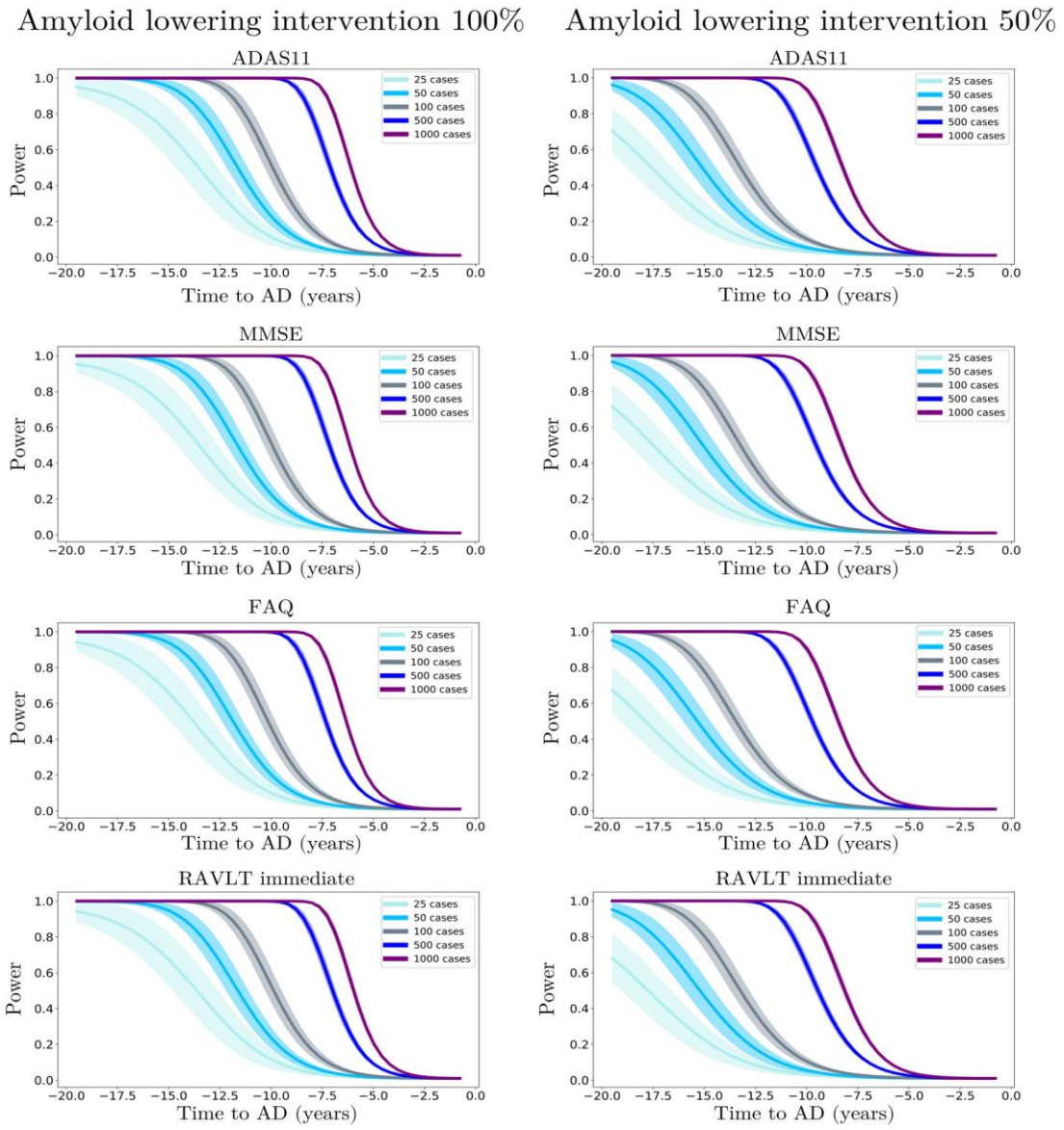

Figure S2. Simulation of sample sizes for clinical trials of an amyloid lowering intervention in cognitively unimpaired participants. Statistical power of the student t-test comparing the estimated clinical outcomes that conversion time between placebo and treated scenarios, according to the year of simulated intervention (100% and 50% amyloid lowering) and sample size for ADAS11, MMSE, FAQ, and RAVLT immediate. Abbreviations: AD, Alzheimer's disease, ADAS11, Alzheimer's Disease Assessment Scale 11 items; FAQ, Functional Activities Questionnaire; MMSE, Mini-Mental State Examination; RAVLT, Rey's Auditory Verbal Learning Test. Reproduced under open access from [2].

A **Variables queried (10):** Mini-Mental State Examination (MMSE), Right Hippocampus Volume, APOE, Geriatric Depression Scale (GDS), AV45 PET, Age, Education, Left Hippocampus Volume, Biological Sex, Clinical Dementia Rating Scale Sum of Boxes (CDRSB)

Cohort (ranked)	Successfully found	Missing features	Number of participants for feature combination	Longitudinal	Modalities	Data access
NACC	10/10 (100.0 %)		1516	Plot	MRI, Clinical, PET, ApoE, Demographics	Apply
A4	10/10 (100.0 %)		1248	Plot	MRI, Clinical, PET, ApoE, Demographics	Apply
ADNI	10/10 (100.0 %)		199	Plot	MRI, Clinical, PET, ApoE, Demographics	Apply
DOD-ADNI	10/10 (100.0 %)		103	Plot	MRI, Clinical, PET, ApoE, Demographics	Apply
EPAD	9/10 (90.0 %)	AV45 PET	1845	Plot	ApoE, Demographics, MRI, Clinical	Apply

B **Longitudinal follow-ups for Mini-Mental State Examination (MMSE), Right Hippocampus Volume, Geriatric Depression Scale (GDS), AV45 PET, Age, Education, Left Hippocampus Volume, Biological Sex, APOE, Clinical Dementia Rating Scale Sum of Boxes (CDRSB) in the NACC cohort.**

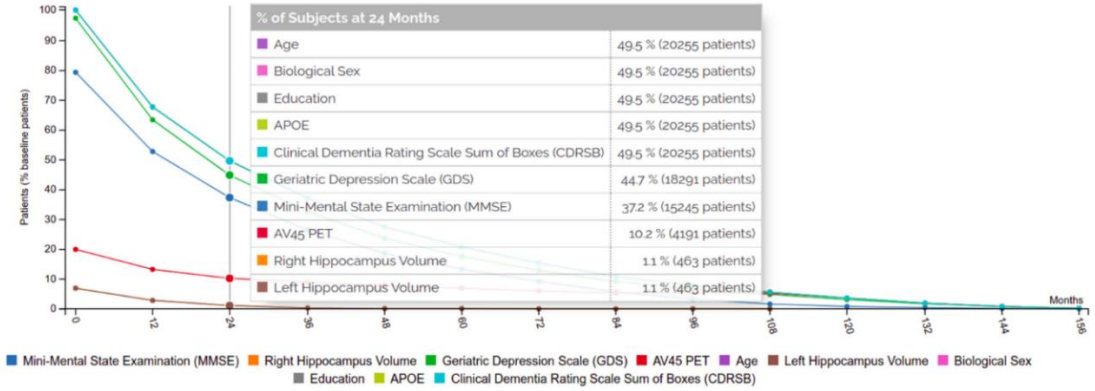

C

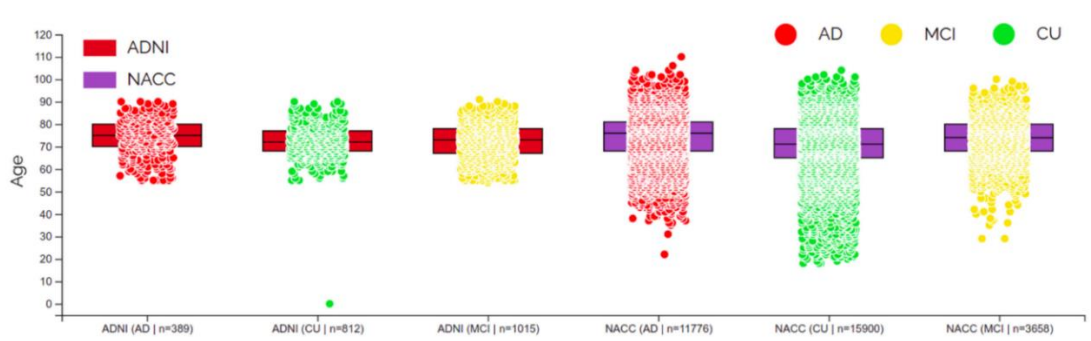

Figure S3. Using ADataViewer to identify suitable cohort data sets. This case scenario aimed to evaluate cognitive decline in the light of depression, AV45 PET, and hippocampal atrophy. All graphs were created using the tools of ADataViewer.(A) Excerpt of the ranking received by entering the variables of interest into the StudyPicker. (B) Longitudinal coverage of specified variables in the NACC cohort. (C) Comparison of the age distributions encountered across diagnostic groups of ADNI and NACC. Abbreviations: NACC, National Alzheimer's Coordinating Center; PET, positron emission tomography. Reproduced under open access from [3].

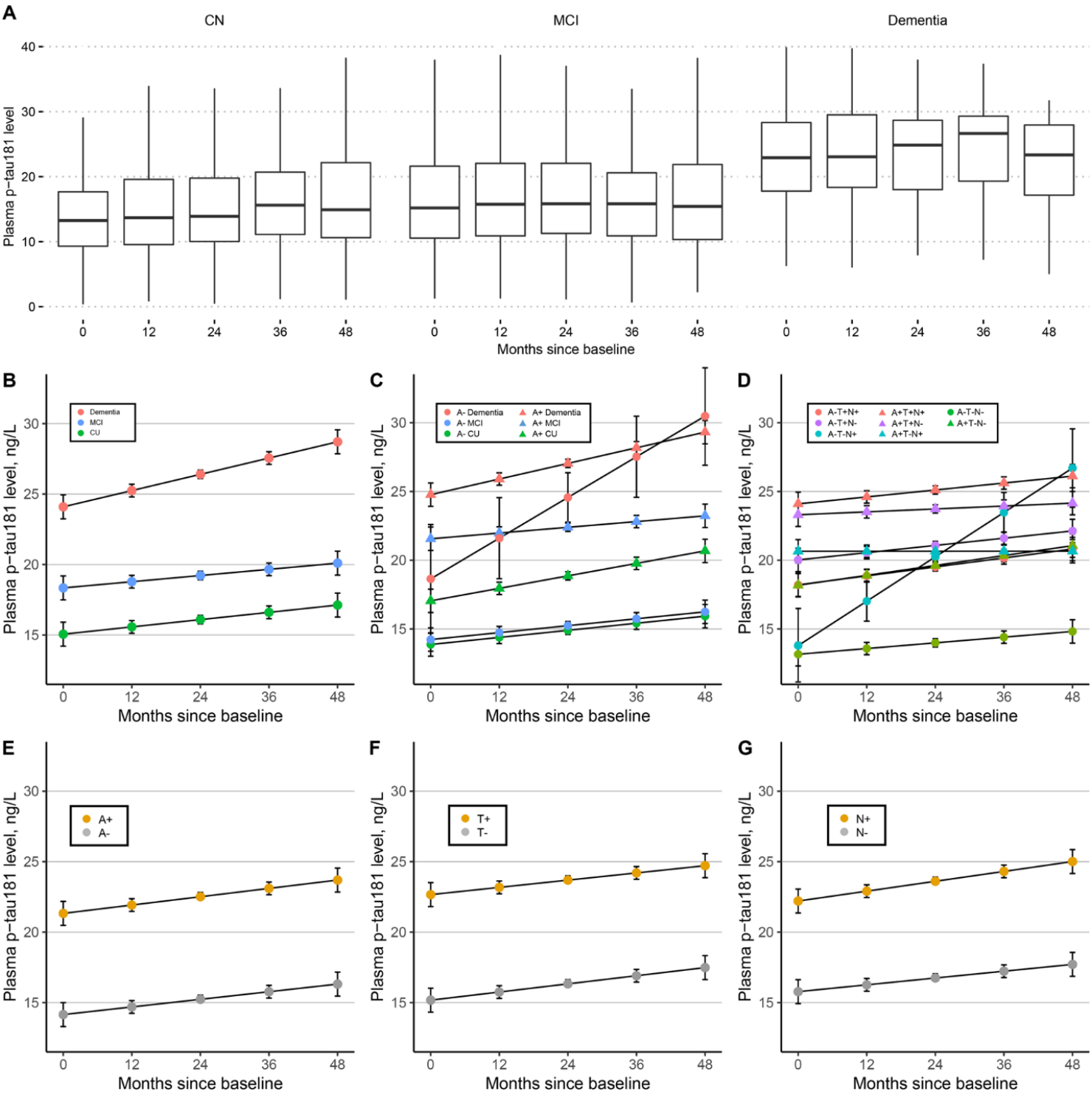

Figure S4. Plasma P-tau181 level by diagnostic group, amyloid status, and ATN classification. (A) Observed data in different diagnostic groups. Estimated plasma P-tau181 trajectories by (B) diagnosis, (C) diagnosis and Aβ status, and (D) ATN classification; Estimated plasma P-tau181 trajectories by (E) *A* status, (F) *T* status, and (G) *N* status. Abbreviations: Aβ, β-amyloid; *A*, amyloid β; CN, cognitively normal; MCI, mild cognitive impairment; *N*, neurodegeneration; *T*, tau. Reproduced under open access from [4].

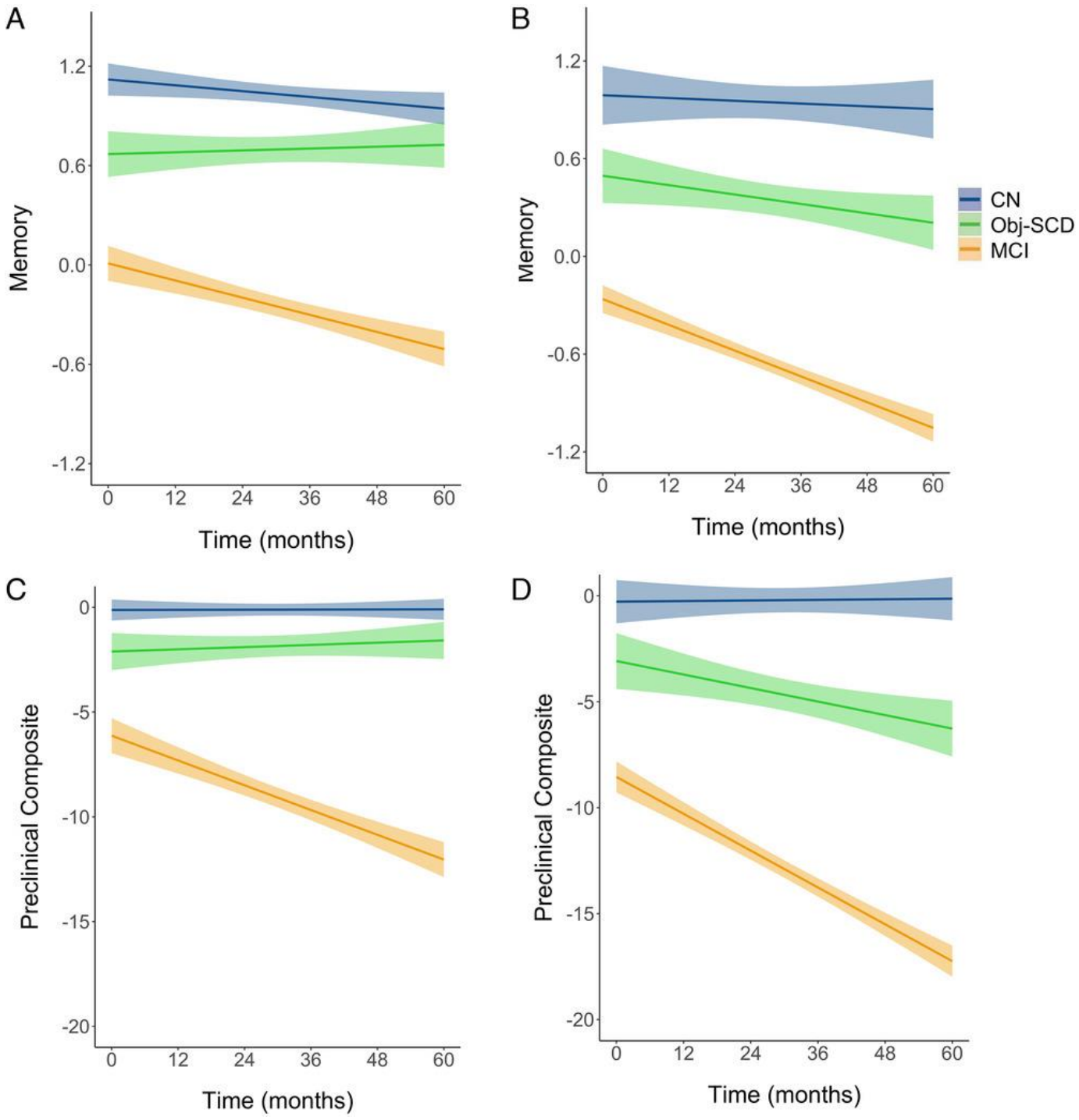

Figure S5. Trajectories of cognitive performance and instrumental activities of daily living (IADL) difficulties by baseline NfL and cognitive group. Predicted performance on the modified Preclinical Alzheimer's Cognitive Composite (mPACC) among those with (A) low baseline NfL and (B) high baseline NfL and mPACC among those with (C) low baseline NfL and (D) high baseline NfL adjusted for age, education, sex, apolipoprotein E (*APOE*) ε4 allele frequency, and p-tau/amyloid β (Aβ) positivity. Shaded area represents 95% confidence intervals. Abbreviations: CN, cognitively normal; MCI, mild cognitive impairment; NfL, neurofilament light; Obj-SCD, objectively-defined subtle cognitive decline. Reproduced under open access from [5].

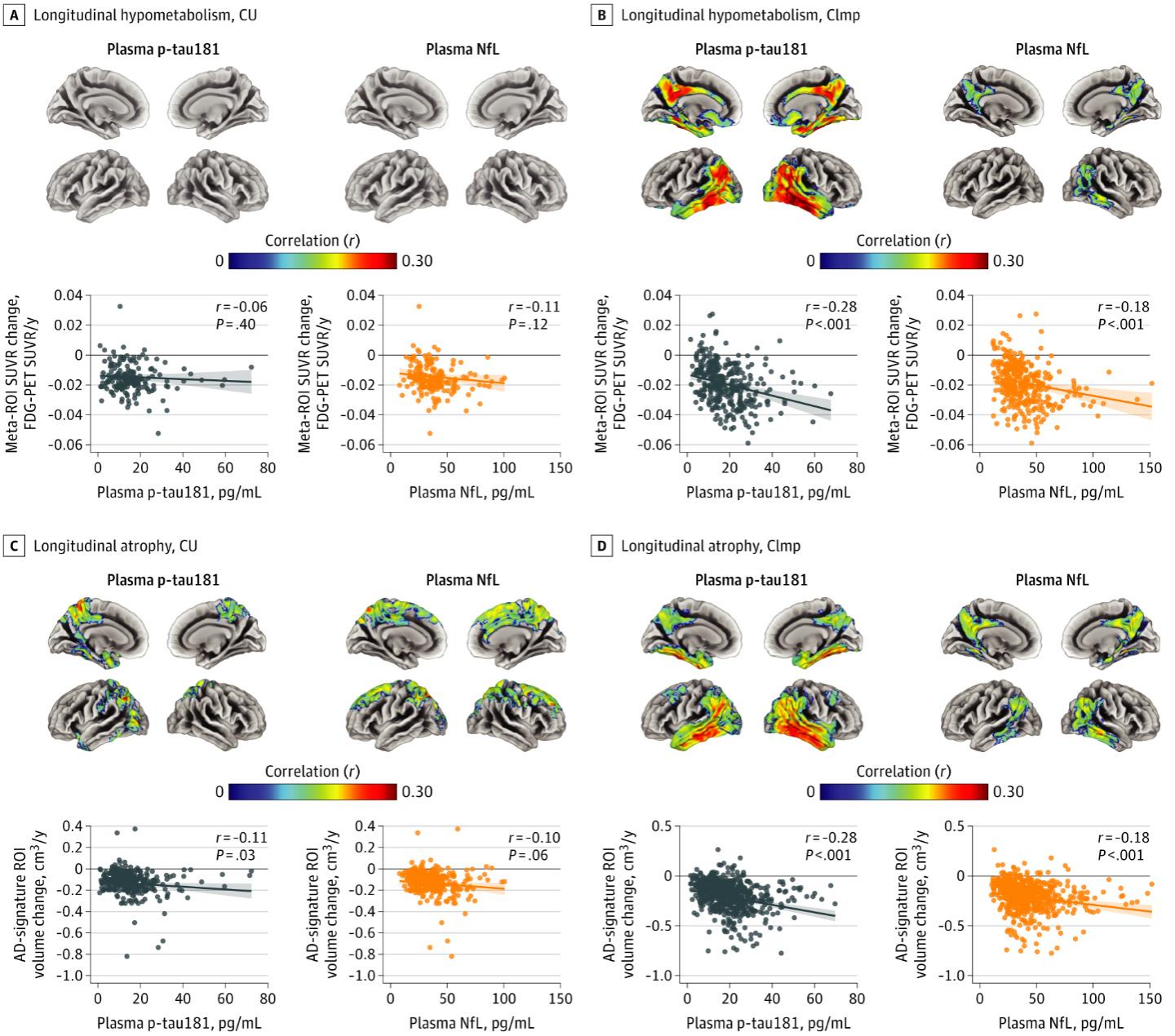

Figure S6. Associations of baseline plasma P-tau181 and neurofilament light with decreasing glucose metabolism and increasing atrophy. Age- and sex-adjusted associations of baseline plasma P-tau181 and NfL with (A) hypometabolism progression in CU, (B) hypometabolism progression in CI, (C) longitudinal atrophy in CU, and (D) longitudinal atrophy in CI. Associations are shown at the voxel (upper row) and Alzheimer disease (AD) meta–ROI level (bottom row). Results of voxelwise analyses were thresholded at P < .01 (uncorrected) for the CU group and at P < .001 (uncorrected) for CImp. All maps were further thresholded at P < .05 (familywise error corrected) at the cluster level. Abbreviations: CI and CImp, cognitively impaired; CU, cognitively unimpaired; P-tau181, tau phosphorylated at 181; FDG PET [18F]-fluorodeoxyglucose positron emission tomography; ROI, region of interest; NfL, neurofilament light; SUVR, standardized uptake value ratio. Reproduced under open access from [6].

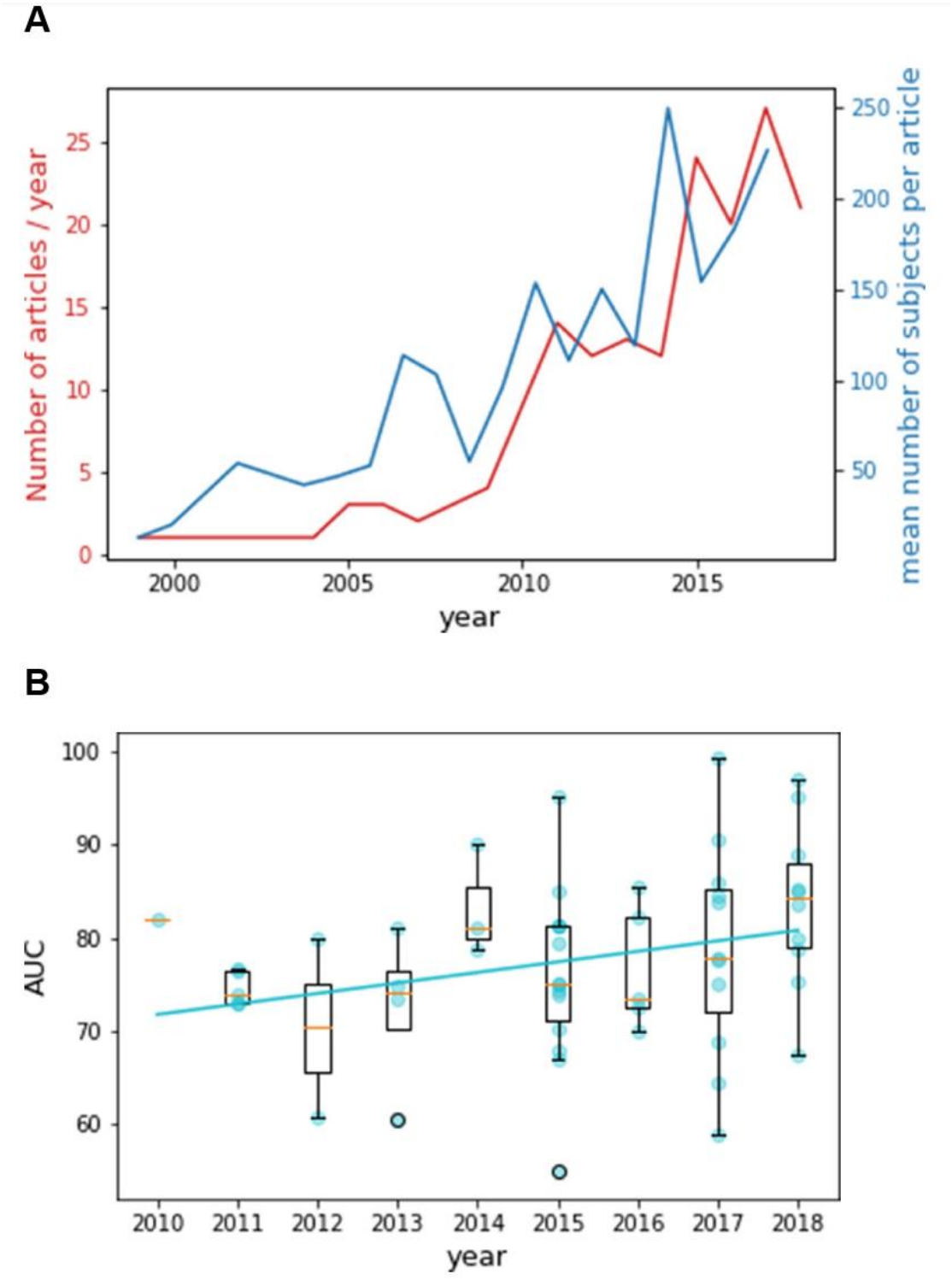

Figure S7. Recent trends in machine learning models predicting MCI progression to AD. (A) Evolution of number of articles per year (in red) and of the number of individuals per article with time (in blue). (B) Evolution of the area under the ROC (receiver operating characteristic) curve (AUC) with time. The AUC of each article is represented by a dot. The AUC of articles published the same year is represented as box-plots. The plain line corresponds to the regression of the AUC against time. Abbreviations: AD, Alzheimer's disease dementia; MCI, mild cognitive impairment. Reproduced under open access from [7].

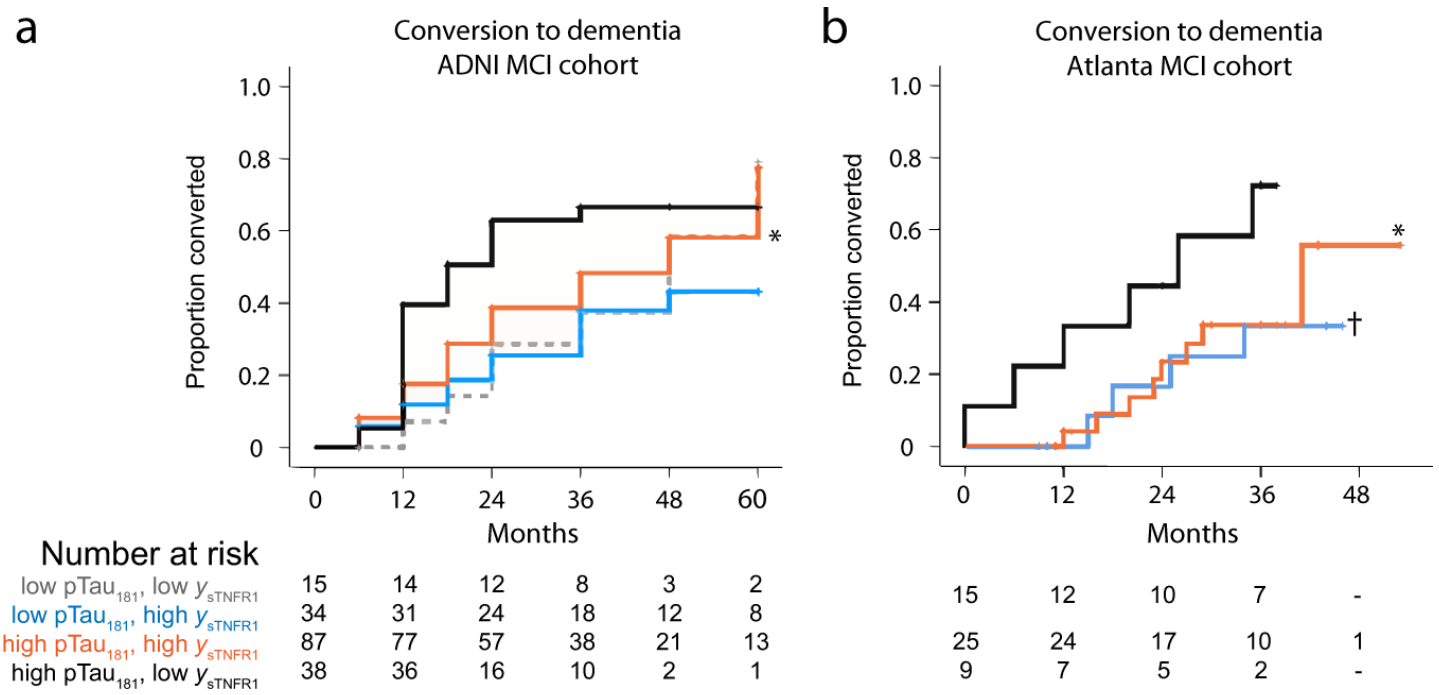

Figure S8. Conversion to dementia diagnosis by CSF P-tau181 and sTNFR1 levels. (A) ADNI (B) Atlanta replication cohort. *Lower conversion compared to those with p-Tau$_{181}$ ≥ 24.1 pg/mL but low y_{sTNFR1} ($p = 0.049$ in ADNI and $p = 0.038$ in the Atlanta cohort).†Two subgroups with p-Tau$_{181}$ < 24.1 were combined due to small numbers, $p = 0.068$ vs. high p-Tau$_{181}$ and low y_{sTNFR1}. Abbreviations: MCI, mild cognitive impairment; sTNFR1, soluble tumor necrosis factor receptor 1. Reproduced under open access from [8].

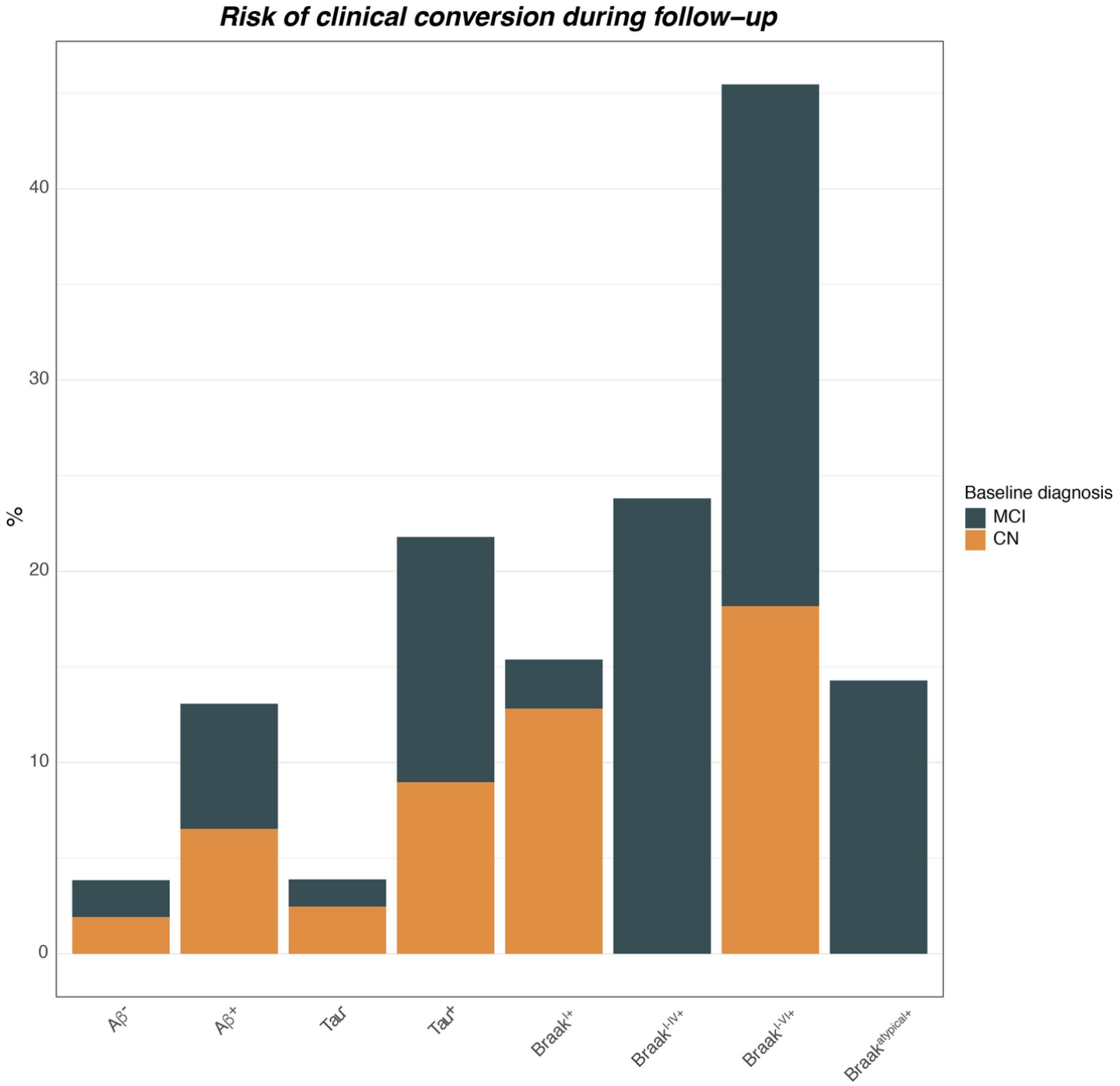

Figure S9. Rates of clinical conversion during follow-up stratified by amyloid-PET positivity, tau-PET positivity and Braak-stage group. Barplots show relative risk of clinical conversion from cognitive normal (CN) to mild cognitive impairment (MCI) or dementia, and from MCI to dementia. Note that subjects with a baseline diagnosis of dementia were excluded from this analysis, since no further diagnostic change can be observed in these participants. Reproduced under open access from [9].

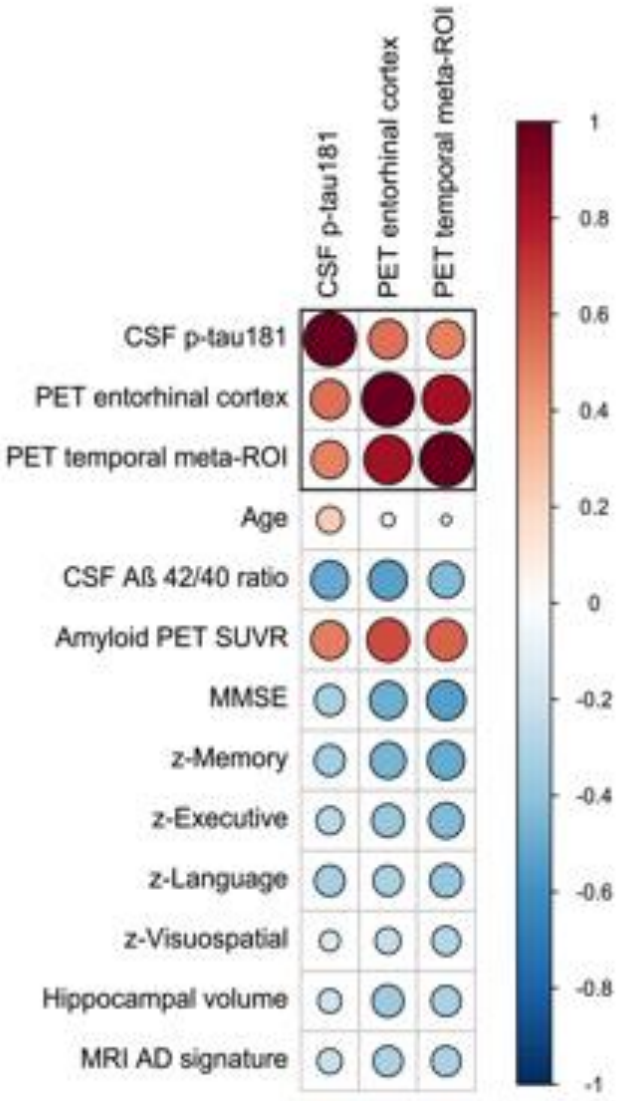

Figure S10. Correlations between tau PET/fluid biomarkers and AD features. Matrix of correlation coefficients between all available tau biomarkers and AD-related features. Strong positive correlations are indicated in dark red, while strong negative correlations indicated in blue. Abbreviations: CSF, cerebrospinal fluid; MMS–E, Mini-Mental State Examination; MRI, magnetic resonance imaging; PET, positron emission tomography; ROI. Region of interest; SUVR, standardized uptake value ratio. Reproduced under open access from[10].

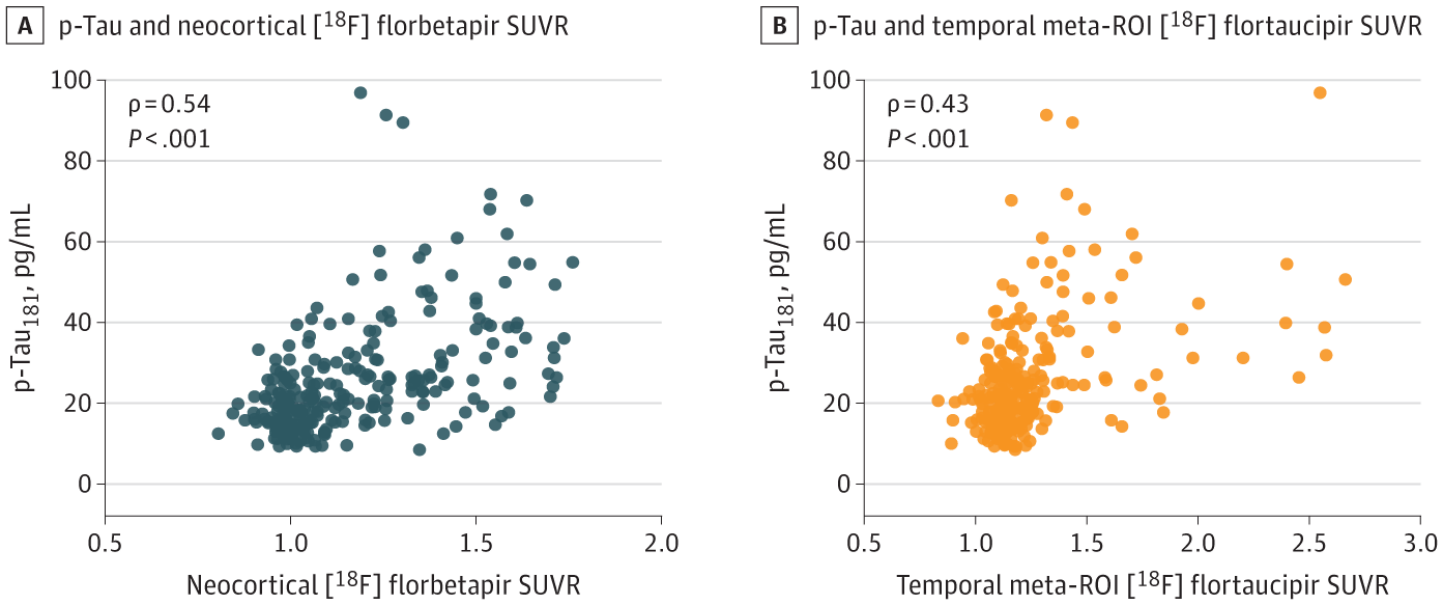

Figure S11. Association between CSF p-tau$_{181}$ and [^{18}F]florbetapir amyloid PET and [^{18}F]flortaucipir tau PET. Abbreviations: ROI, region of interest; SUVR, standardized uptake value ratio. Reproduced under open access from [11].

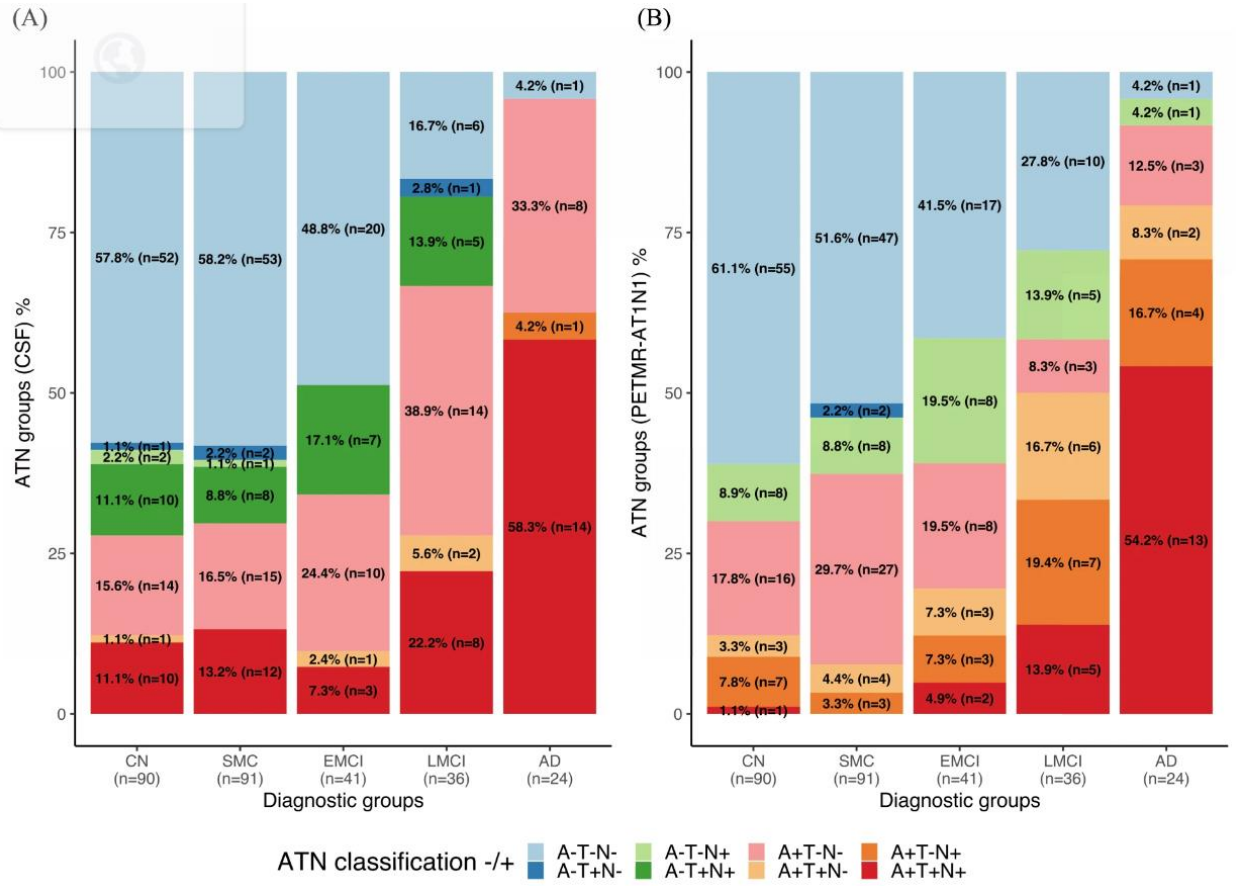

Figure S12. Lack of concordance between ATN profiles defined by CSF biomarkers versus imaging biomarkers by diagnostic group. (A) CSF biomarker results. (B) Imaging biomarker results. Abbreviations: AD, Alzheimer's disease; CN, cognitively normal; EMCI, early MCI; LMCI, late MCI; MCI, mild cognitive impairment; SMC, subjective memory concern. Reproduced under open access from[12].

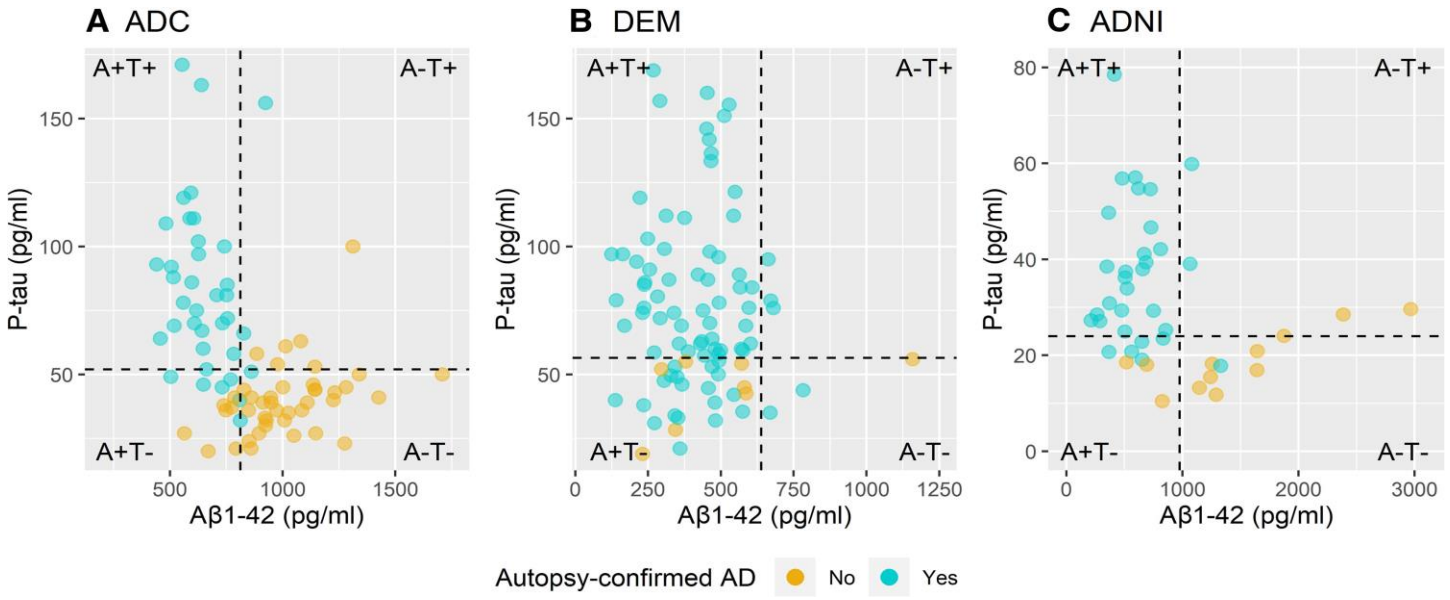

Figure S13. Neuropathological confirmation of AD and biomarker AT (CSF Aβ42 and P-tau181) classification. (**A**) Amsterdam Dementia Cohort (ADC), (**B**) Antwerp Dementia Cohort (DEM) and (**C**) ADNI. The dotted vertical lines correspond to the $A\beta_{1\text{-}42}$ cutoffs of <813 pg/ml for ADC, <638.5 pg/ml for DEM and <977 pg/ml for ADNI. The dotted horizontal lines correspond to the p-tau cutoffs of >52 pg/ml for ADC, >56.5 pg/ml for DEM and >24 pg/ml for ADNI. Reproduced under open access from[13].

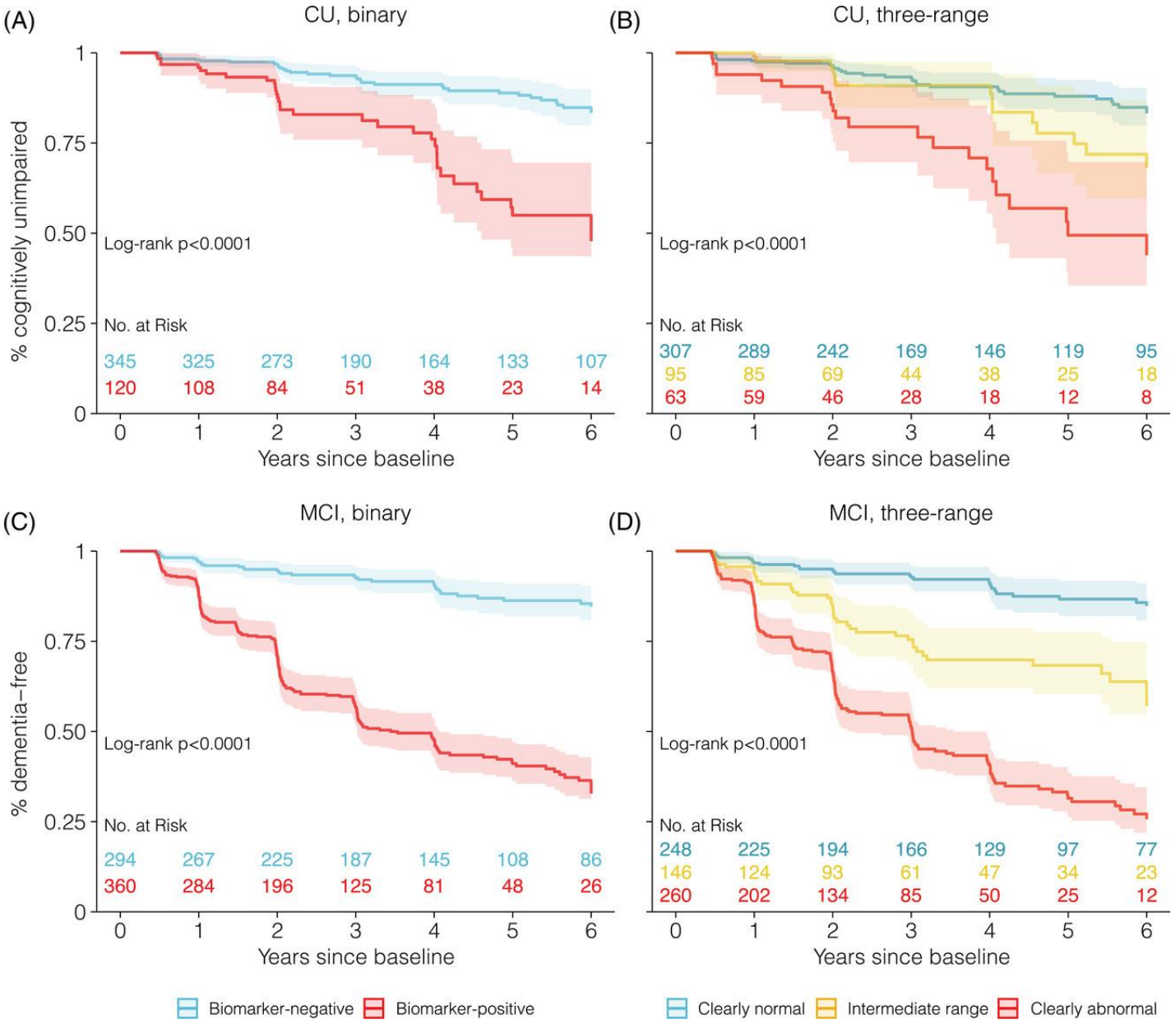

Figure S14. Kaplan-Meier curves and the risk of onset of cognitive impairment or dementia according to binary and three range of CSF P-tau181/Aβ42 cutpoints. Kaplan-Meier curves for survival analysis predicting clinical progression according to CSF P-tau181/Aβ42 baseline status. Survival curves are displayed for the conversion from CU to MCI according to (A) binary and (B) three range cutpoints. For MCI to dementia, they are displayed according to (C) binary or (D) three range biomarker status. The previously described binary cut point of 0.0251 was used for CSF P-tau181/Aβ42 ratio, whereas derived cutpoints (0.023; 0.0377) were used for the three range group. Abbreviations: CSF, cerebrospinal fluid; CU, cognitively unimpaired; MCI, mild cognitive impairment; mPACC, modified Preclinical Alzheimer's Cognitive Composite. Reproduced under open access from [14].

Veitch et al. The Alzheimer's Disease Neuroimaging Initiative in the era of Alzheimer's disease treatment

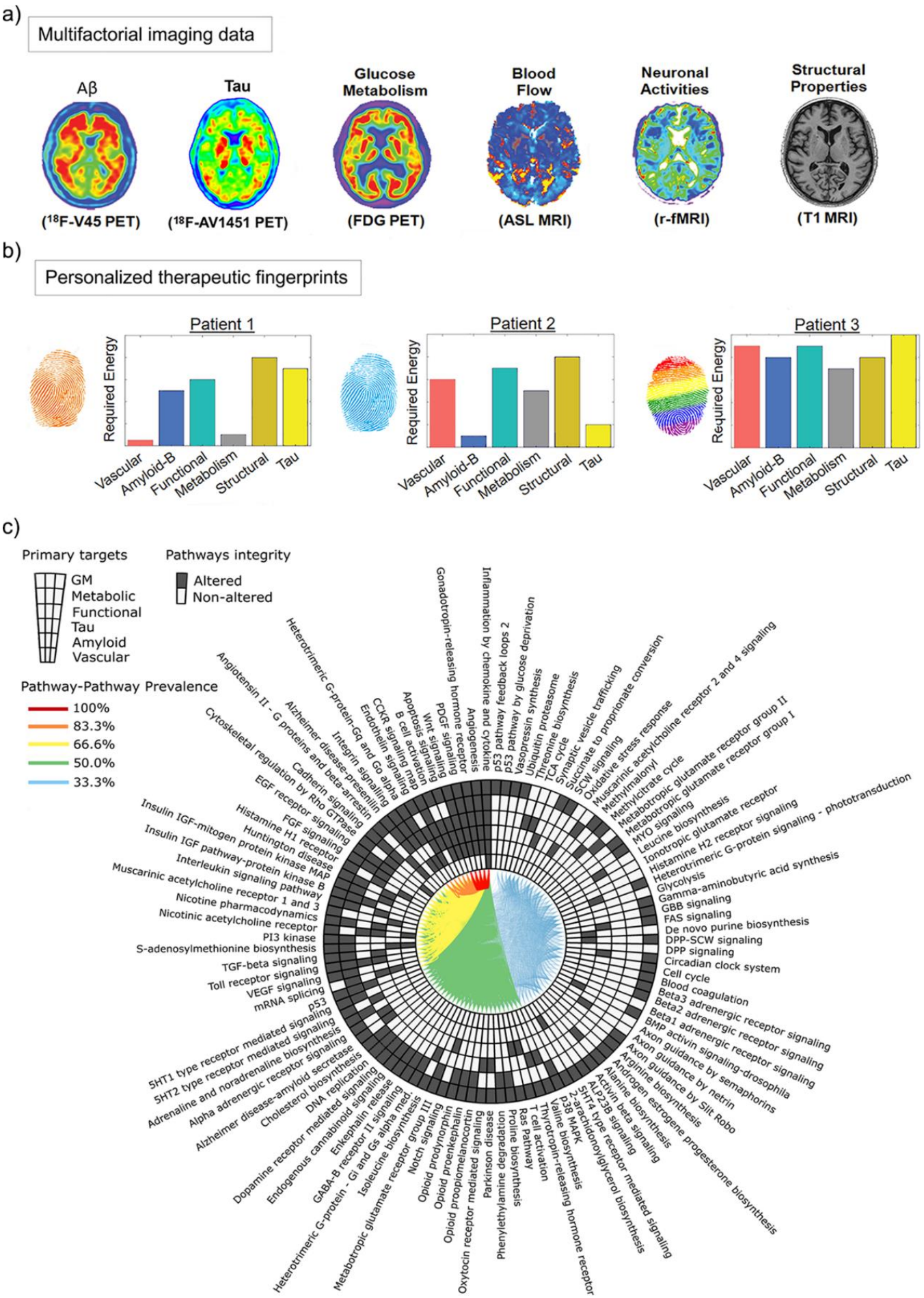

Figure S15. The *NeuroPM*-box software tool for biologically stratifying participants. (A) Imaging for amyloid, tau, glucose metabolism, cerebral blood flow, neuronal activity at rest, and gray matter density. Using a network-based approach, the personalized therapeutic individual fingerprint (pTIF) enables individual characterization of the direct factor-to-factor intra-brain biological interactions and the multifactorial spreading mechanisms through vascular/anatomical connections. (B) Dissimilar pTIF patterns for three participants with the same diagnosis. Patient 1 requires low-cost vascular and metabolic interventions and Patient 2 requires low-cost interventions for anti-Aß and anti-tau interventions, suggesting different single-target therapies could benefit both patients (e.g., physical exercise and aducanumab, respectively). However, Patient 3 requires multiple single-target interventions, suggesting that a high-cost combinatorial treatment, as opposed to a single-target treatment, would be more beneficial for this patient. (C) The altered molecular pathways (blood data) underlying the distinct single-target therapeutic needs. Starting at 12 o'clock and moving counter-clockwise, the pathways for each of the single-target subgroups were sorted according to prevalence. Each link between a given pair of pathways corresponds to the percentage of subgroups for which molecular pathways were found to be affected. Abbreviations: ASL, arterial spin labeling; FDG PET, fluorodeoxyglucose, positron emission tomography; GM, gray matter; MRI, magnetic resonance imaging; rs-fMRI, resting state functional MRI. Reproduced under open access from[15].

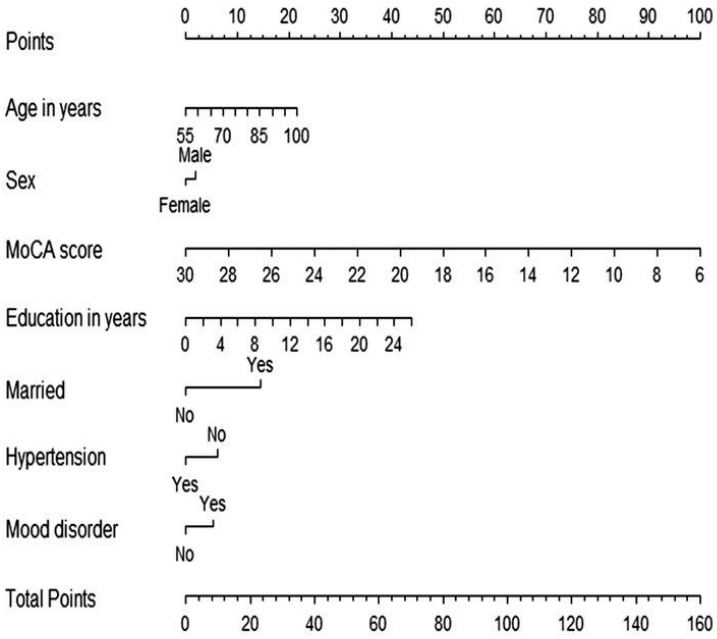

Age in years	Points
55	0
60	2
65	5
70	7
75	10
80	12
85	14
90	17
95	19

Sex	Points
Female	0
Male	2

MoCA	Points
14	67
16	58
18	50
20	42
22	33
24	25
26	17
28	8
30	0

Education (in years)	Points
12	21
16	30
20	34
25	42

Hypertension	Points
Yes	0
No	6

Married/common-law	Points
Yes	14
No	0

Mood disorder	Points
Yes	5
No	0

3-year risk of dementia	Total points
90%	122
80%	113
70%	105
60%	99
50%	92
40%	84
30%	75
20%	63
10%	44

Figure S16. Point system for nomogram for CIDER dementia risk score using MoCA. Abbreviations: CIDER, mild Cognitive Impairment to DEmentia Risk; MoCA, MOntréal Cognitive Assessment. Reproduced under open access from[16].

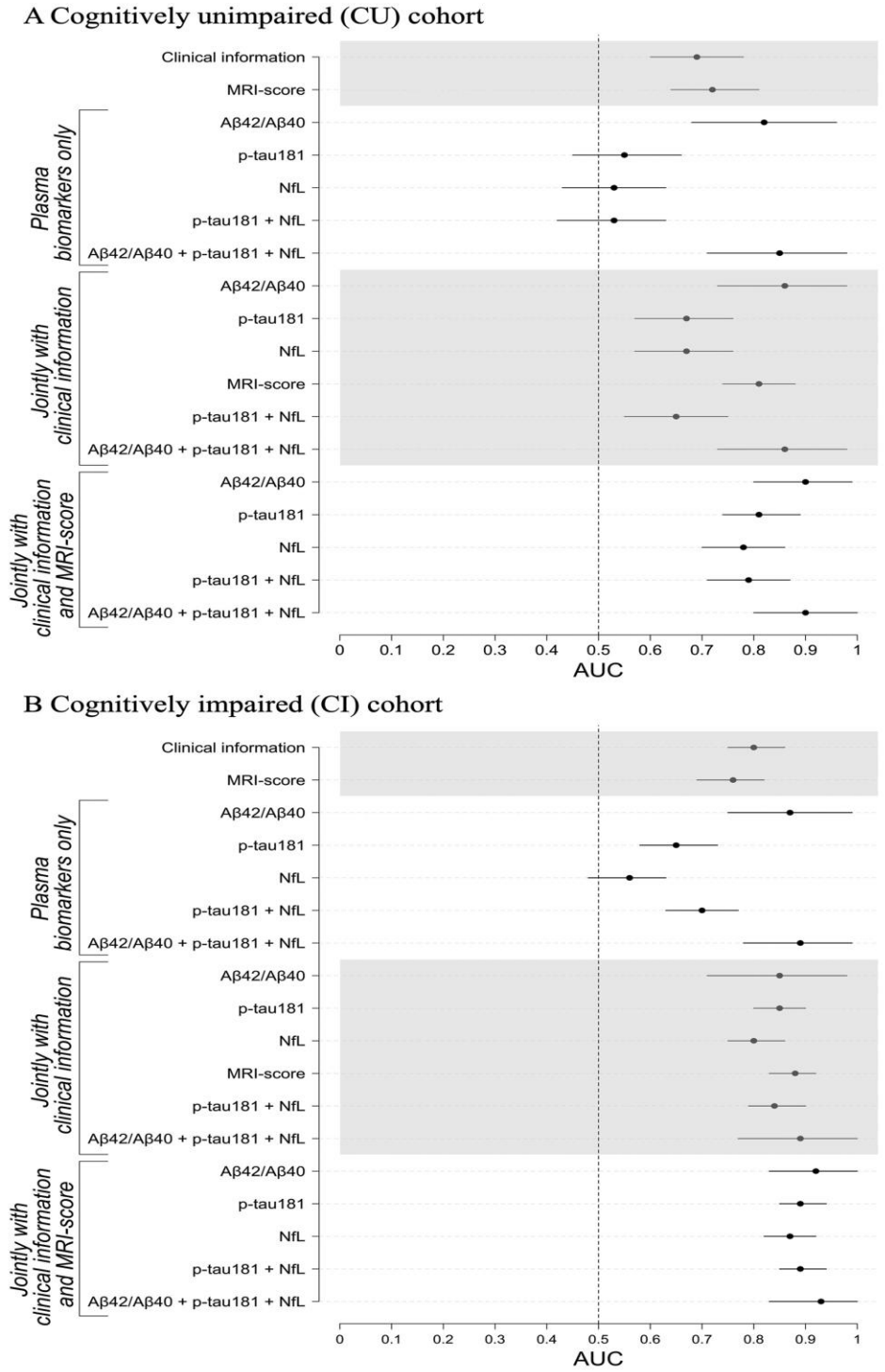

Figure S17. Prediction of amyloid (Aβ) positivity using plasma biomarkers, clinical information, and MRI. Classifier performance metrics of Aβ positivity prediction in (A) cognitively unimpaired (CU) individuals and B) individuals with mild cognitive impairment (CI). Area under the curve (AUC) are shown for classifiers constructed separately and jointly with demographic information (age, sex and years of education), *APOE*, clinical scores, plasma biomarkers (Aβ42/Aβ40, p-tau181 and NfL) and structural MRI-score when predicting Aβ-positivity using florbetapir PET as the ground truth. Error bars indicate union of 95% CIs from cross-validation iterations. Abbreviations: MRI, magnetic resonance imaging; NfL. neurofilament light. Reproduced under open access from[17].

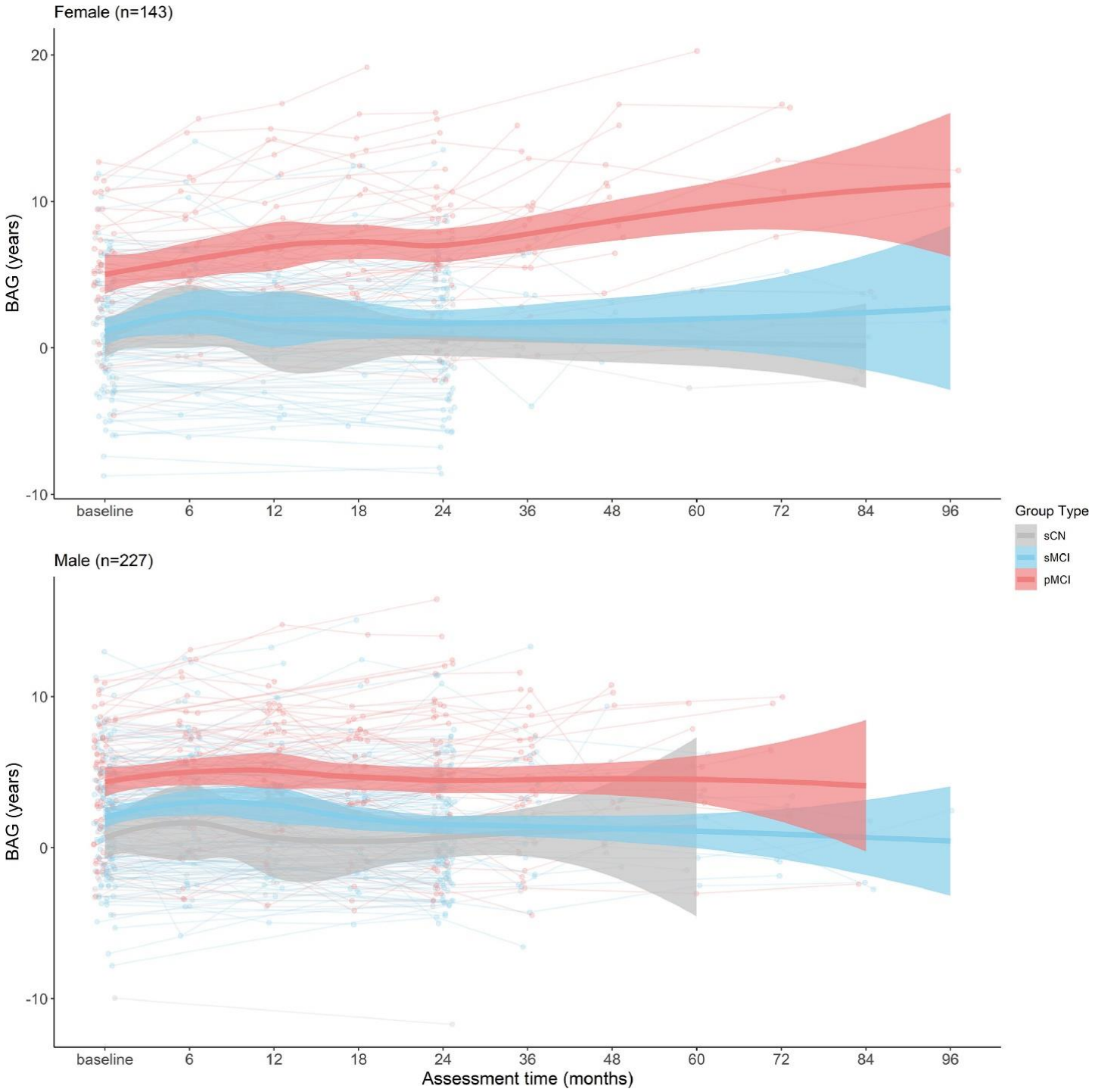

Figure S18. Individual and group brain age gap (BAG) values at each assessment month following baseline. Top - females. Bottom – males. Thick lines represent BAG of all subjects for each group across assessments. Shaded area along each curve indicates the 95% confidence interval. Individual dots and lines represent individual subjects for each group. Groups are given as stable cognitively normal (sCN), stable mild cognitive impairment (sMCI), and progressive mild cognitive impairment (pMCI). Assessment time represents the months following the baseline (initial) assessment. Reproduced under open access from [18].

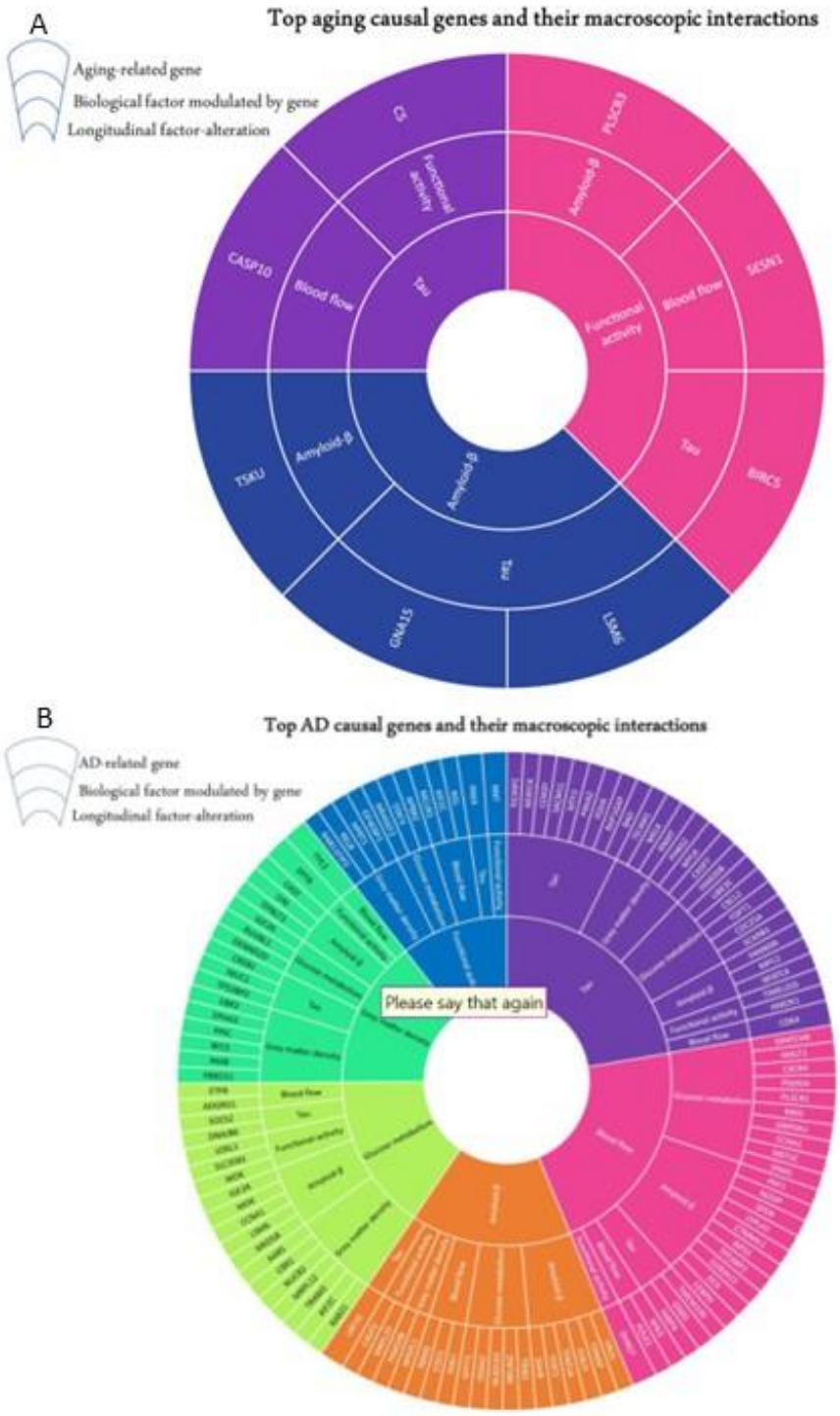

Figure S19. Identification of top genetic determinants of cognitive change in healthy aging, and in AD progression. (A) Top genetic determinants of multifactorial alterations in healthy aging. (B) Top genetic determinants of AD progression. The innermost ring shows the longitudinal biological factors altered with aging or AD, the middle ring shows the interacting biological factors driving the longitudinal operation, and the outermost ring represents the causal genes modulating the interactions among biological factors. Reproduced under open access from [19].

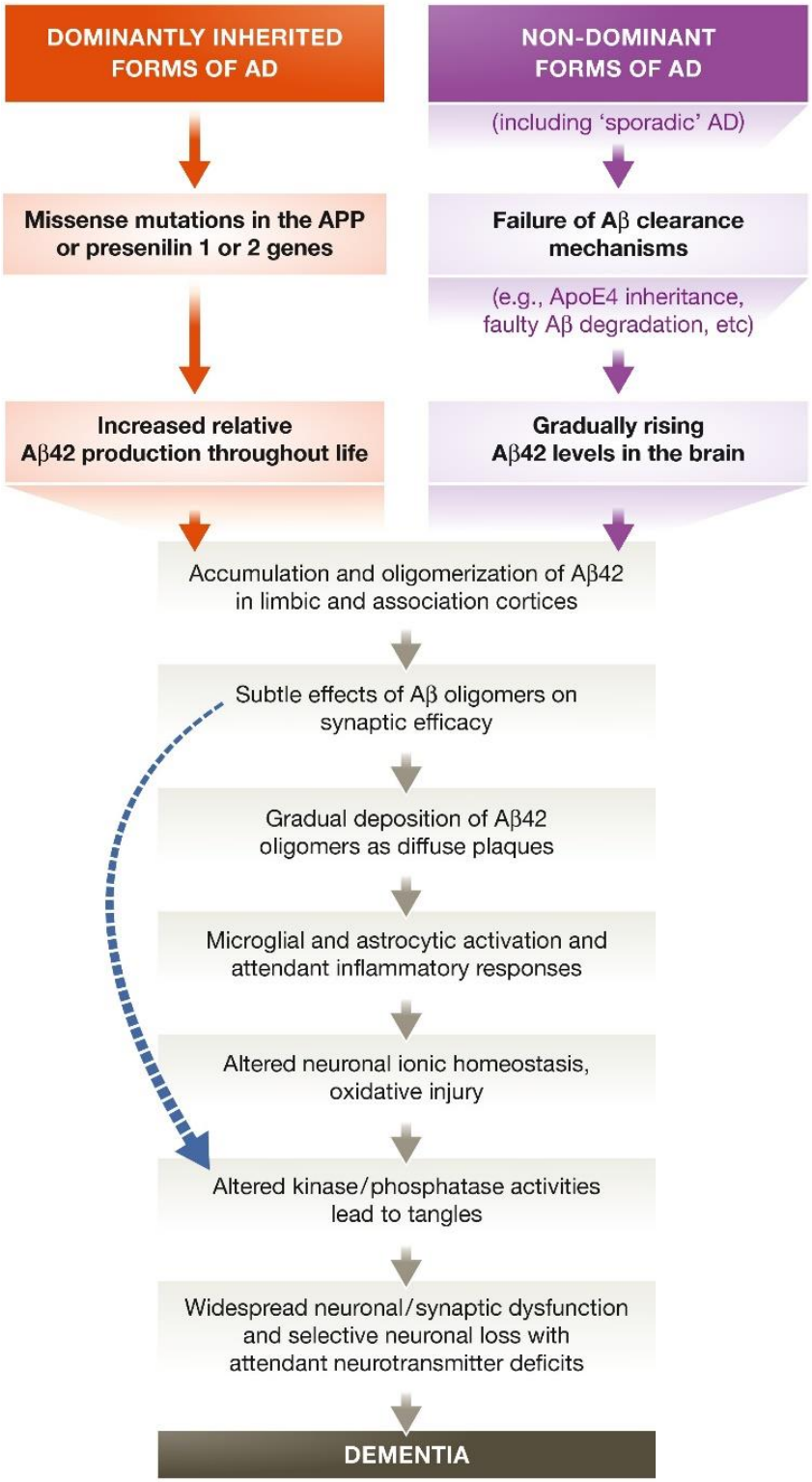

Figure S20. The sequence of major pathogenic events leading to AD proposed by the amyloid cascade hypothesis. The curved blue arrow indicates that Aβ oligomers may directly injure the synapses and neurites of brain neurons, in addition to activating microglia and astrocytes. Reproduced under open access from [20].

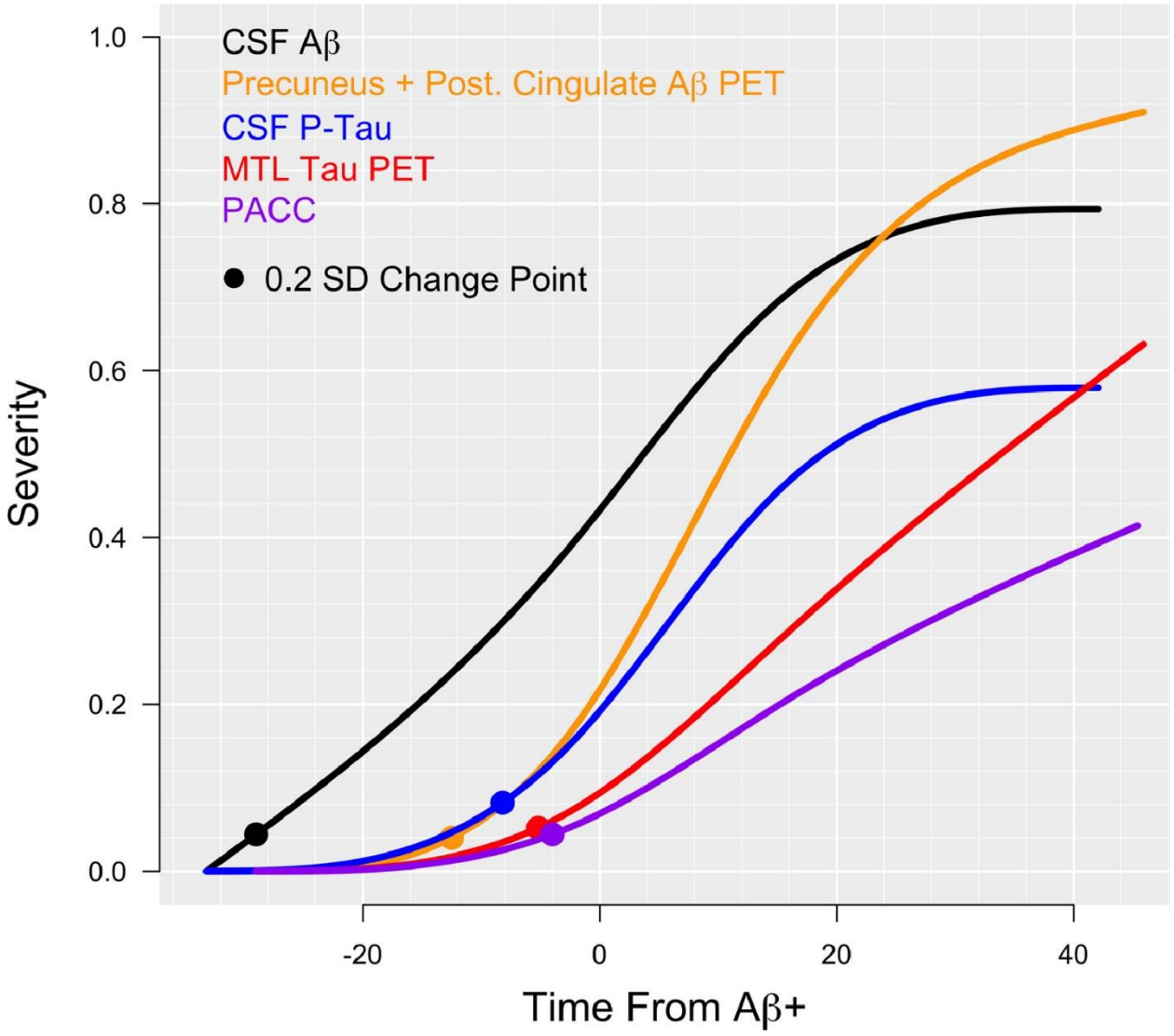

Figure S21. Summary curves for the estimated time to amyloid positivity. Summary curves are shown for all modalities on a scale from zero to one. Responses are scaled such that zero is the least pathological point for each response and one is the mean response in the AD participants. The initial effect, defined by 0.2 SD change points are plotted. Abbreviations: CSF, cerebrospinal fluid; MTL, medial temporal lobe; PACC, Preclinical Alzheimer's Cognitive Composite; PET, positron emission tomography. Reproduced under open access from [21].

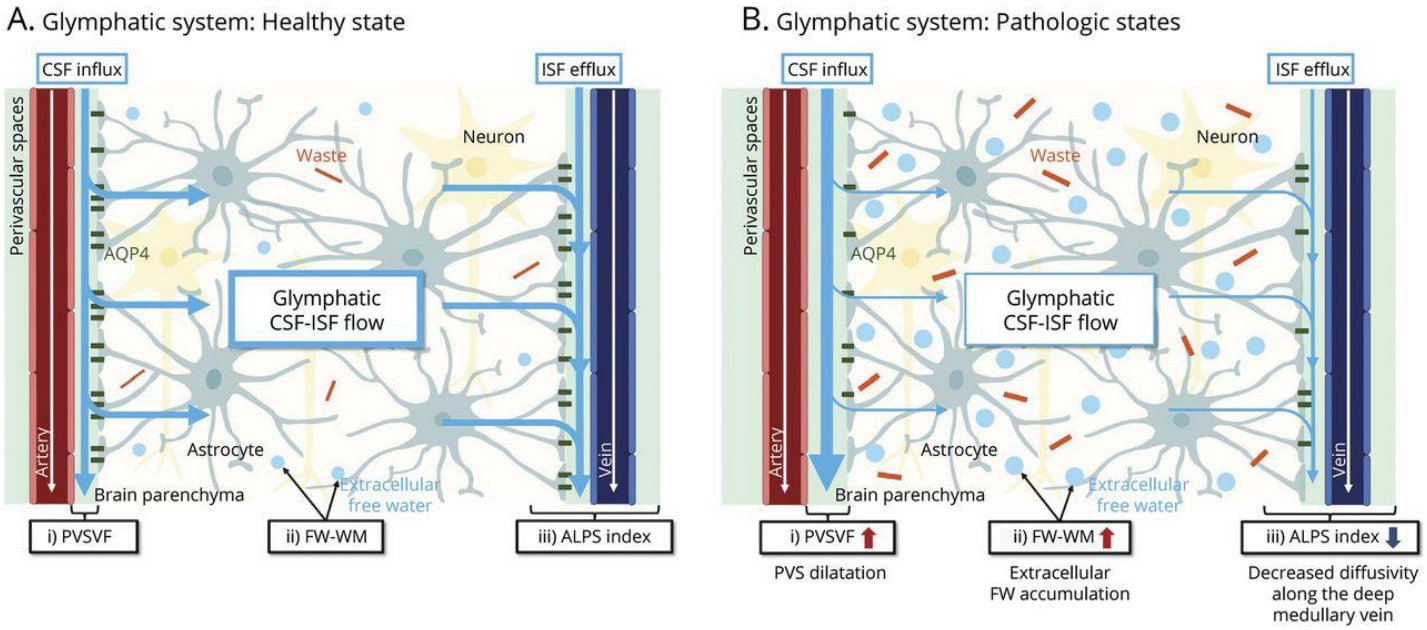

Figure S22. Lymphatic system compartments in healthy and pathological states. (A) Based on the lymphatic hypothesis, subarachnoid CSF normally enters the brain's interstitial space from the periarterial space through the aquaporin channel in the astrocytic end-feet and then mixes with interstitial fluids (ISF) and waste solutes in the brain. The resulting exchange between CSF/ ISF and waste products, such as Aβ, are then drained out of the brain by the paravenous efflux pathway. (B) In the pathologic state, such as in Alzheimer's disease, lymphatic dysfunction due to brain waste (i.e. Aβ) accumulation might cause enlargement of the perivascular space, increased brain extracellular free water, and decreased perivenous efflux. MRI measures of these effects are indicated. Abbreviations: ALPS, diffusivity along the perivascular space; AQP4, aquaporin; CSF, cerebrospinal fluid; FW-WM, free water in the white matter; PVS, perivascular space; PVSVF, PVS volume fraction. Reproduced under open access from[22].

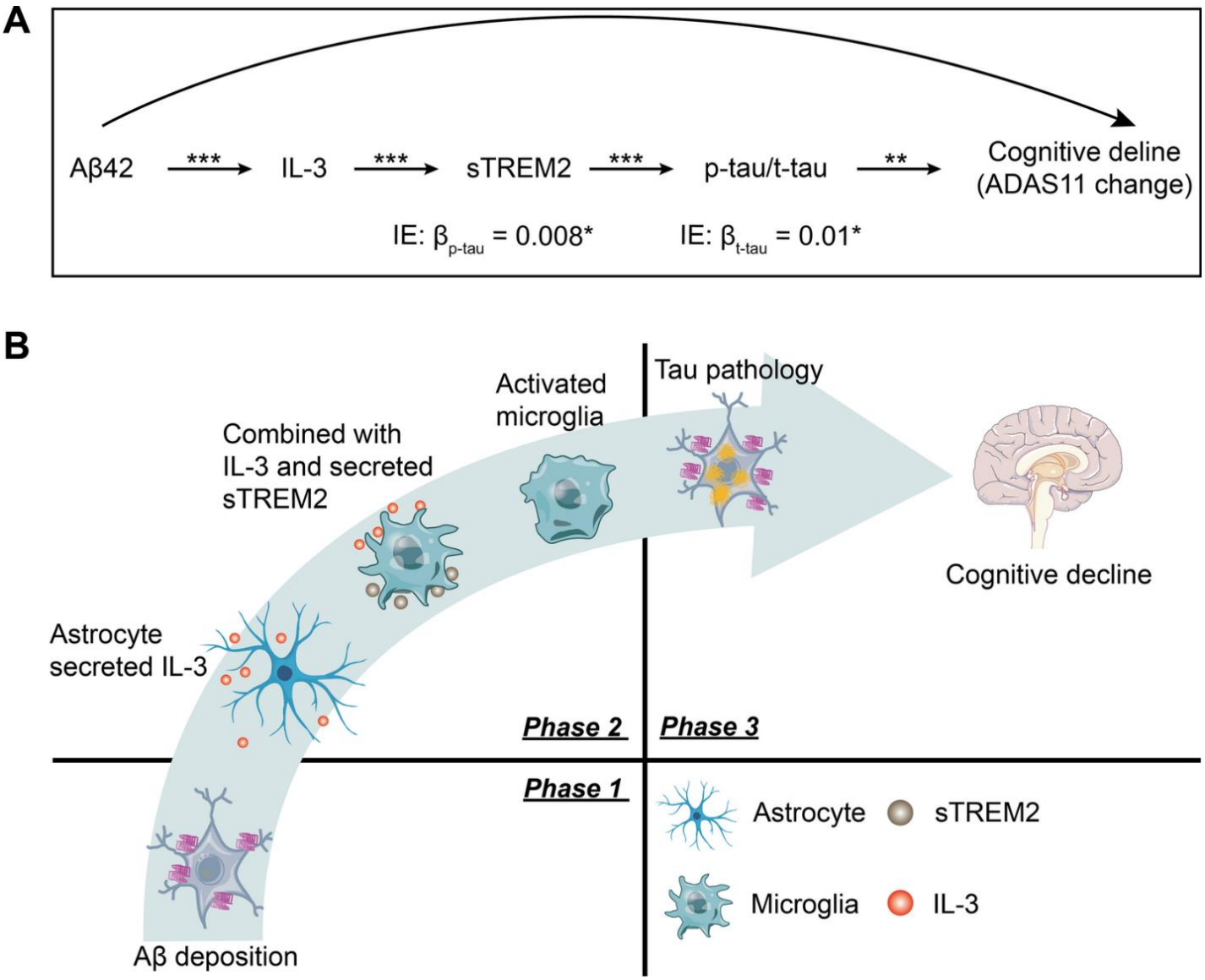

Figure S23. Schematic representation of crosstalk between interleukin-3 and soluble TREM2. (A) The mediation analysis was explored between Aβ42 and ADAS11 annual change: Aβ42 → IL-3 → sTREM2 → p-tau/t-tau → ADAS11 change. $^{*}P < 0.05$,$^{**}P < 0.01$ and $^{***}P < 0.001$. (B) Schematic representation of the effect of astrocyte–microglia communication on progression of AD pathogenesis. Aβ deposition is the initial step during the development of AD pathogenesis. As the compensative pathway, astrocytes can secrete IL-3 to activate microglia to secrete sTREM2, which leads to microglial activation to clear Aβ deposition. However, when their functions are not powerful enough to remove Aβ deposition, tau-related pathology and neuronal loss will occur, resulting in cognitive decline. Abbreviations: Aβ, amyloid β; ADAS11, Alzheimer's Disease Assessment Scale 11; IL-3, interleukin -3; sTREM2, soluble triggering receptor expressed on myeloid cells. Reproduced under open access from [23].

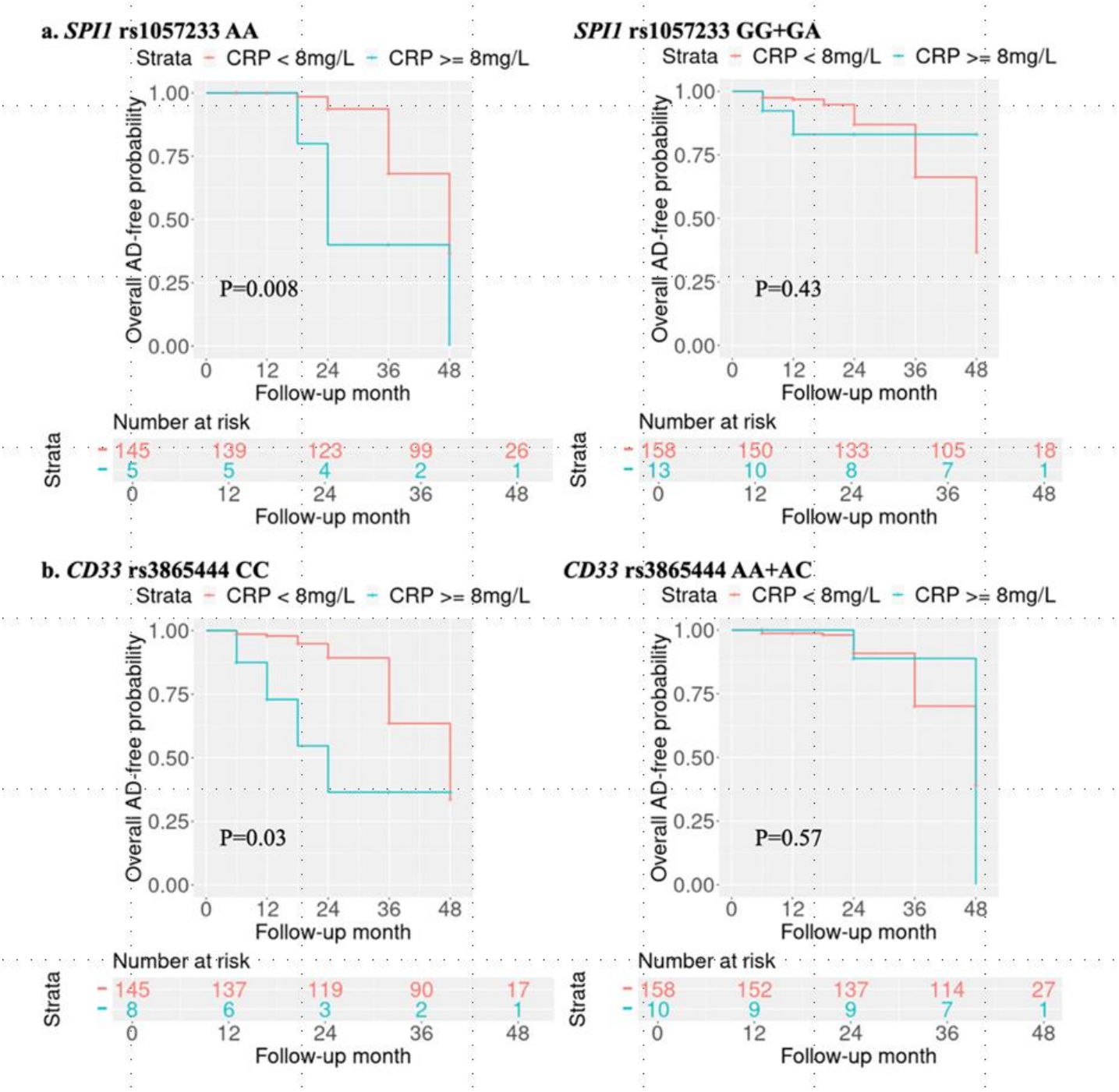

Figure S24. Kaplan-Meier survival plots for the stratified *SPI1* and *CD33* genotypes for the effect of C-reactive protein levels on MCI to AD conversion. ADNI MCI participants were stratified by genotypes. Kaplan–Meier survival plots were generated for AD free time for *SPI1* rs1057233 and *CD33* rs3865444 genotypes; Red: CRP < 8 mg/L, Green: CRP ≥ 8 mg/L. Abbreviations: AD, Alzheimer's disease.; CRP, C-reactive protein; MCI, mild cognitive impairment. Reproduced under open access from [24].

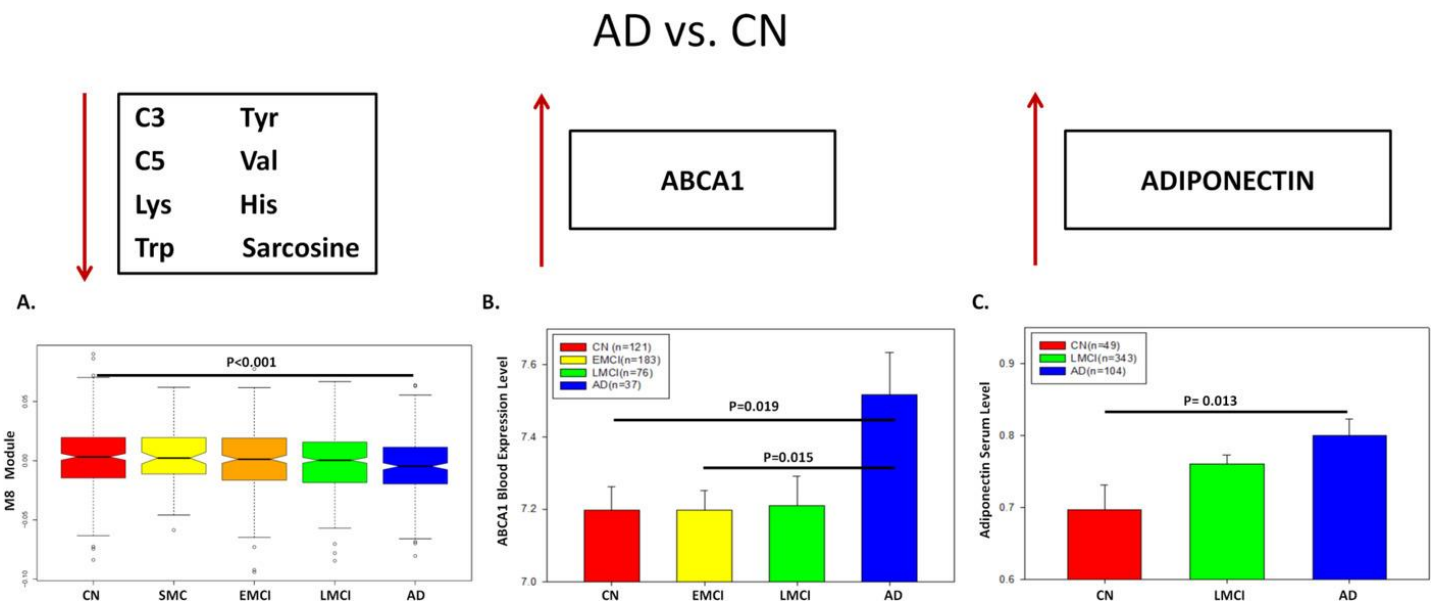

Figure S25. Metabolite coexpression networks and their genetic regulators in relation to AD disease progression. (A) The expression level of the module M8 containing short chain acylcarnitines and amino acids across diagnostic groups. (B) mRNA levels of ABCA1 in blood across diagnostic groups. (C) Adiponectin protein levels in the blood across diagnostic groups. * *P*-value <0.05. Abbreviations: AD, Alzheimer's disease; C3, propionylcarnitine; C5, valerylcarnitine, CN, cognitively unimpaired; EMCI, early mild cognitive impairment; His, histidine; Lys, lysine; LMCI, late mild cognitive impairment; MCI, mild cognitive impairment; Trp, tryptophan; Tyr, tyrosine; Val, valine. Reproduced under open access from [25].

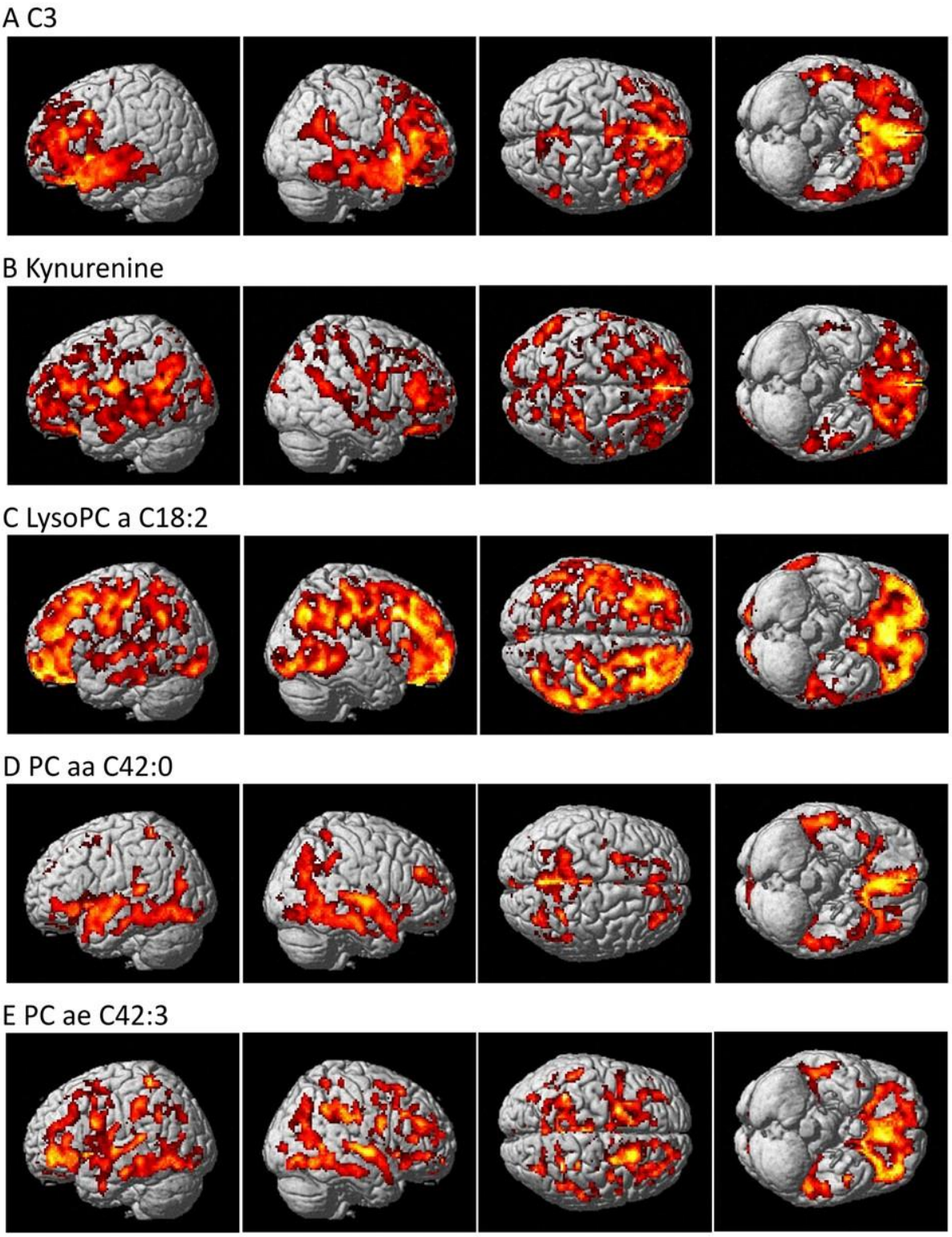

Figure S26. Association of serum metabolites with global amyloid burden. Whole-brain voxel-based imaging analysis for Aβ accumulation using [^{18}F]florbetapir PET scans showing that associations of higher levels of (A) C3 and (B) kynurenine were associated with decreased amyloid-β accumulation, and that higher levels of (C) lysoPC a C18:2, (D) PC aa C42:0 and (E) PC ae C42:3 with increased amyloid-β accumulation (corrected *P*-value < 0.05). Abbreviations: C3, propionylcarnitine; PC, phosphatidylcholine; PET, positron emission tomography. Reproduced under open access from [26].

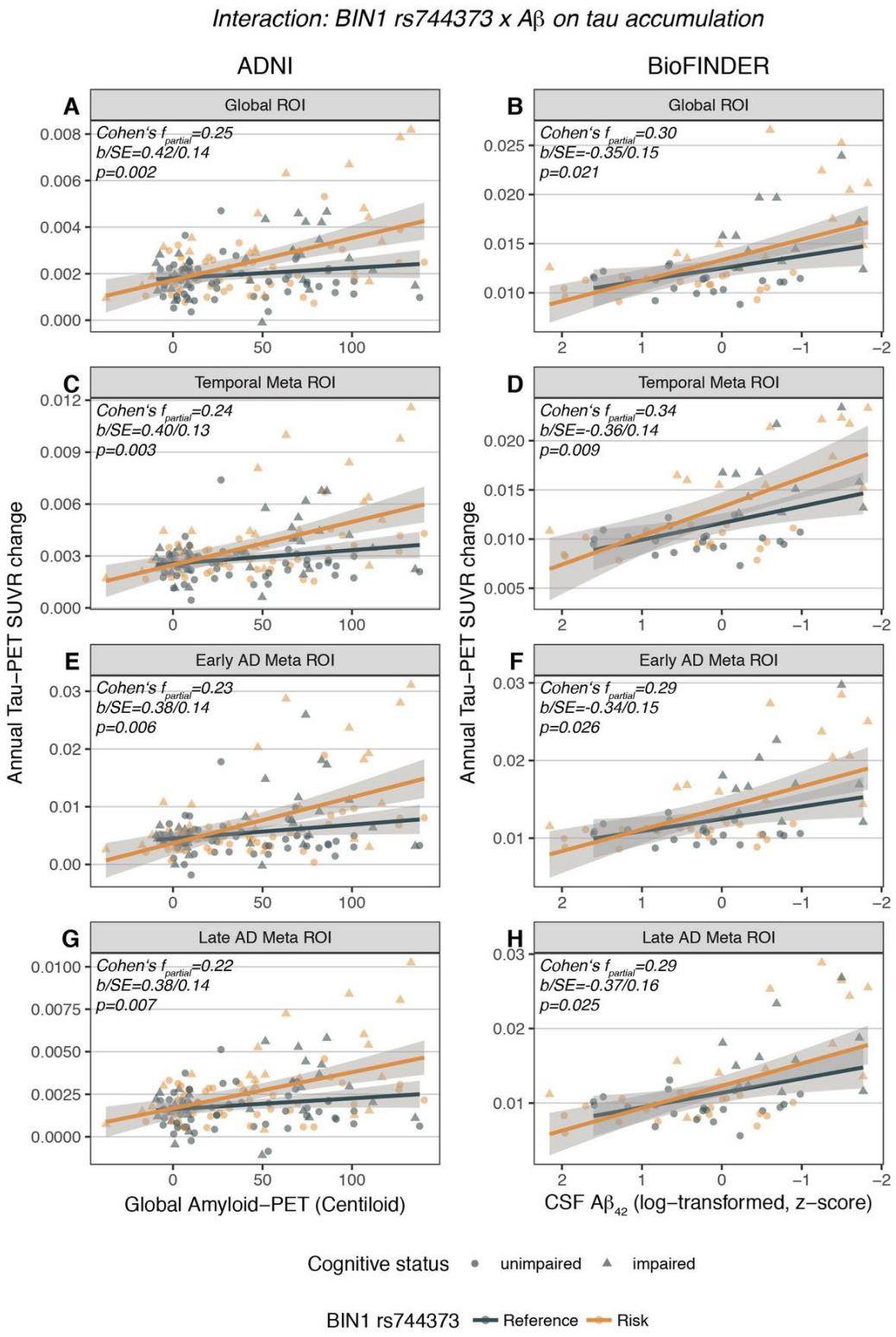

Figure S27. Interaction effects for the *BIN1* rs 744373 by amyloid β on tau accumulation rates. *P*-values indicate significance of interaction effects and were derived from linear regression models controlling for age, sex, education, *APOE* ε4 status, maximum follow-up duration, diagnosis, and baseline tau levels of the respective regions of interest (ROIs). Gray shaded areas indicate standard errors of the regression bars. Abbreviations: AD, Alzheimer's disease; PET, positron emission tomography; ROI, region of interest; SUVR, standardized uptake value ratio. Reproduced under open access from [27].

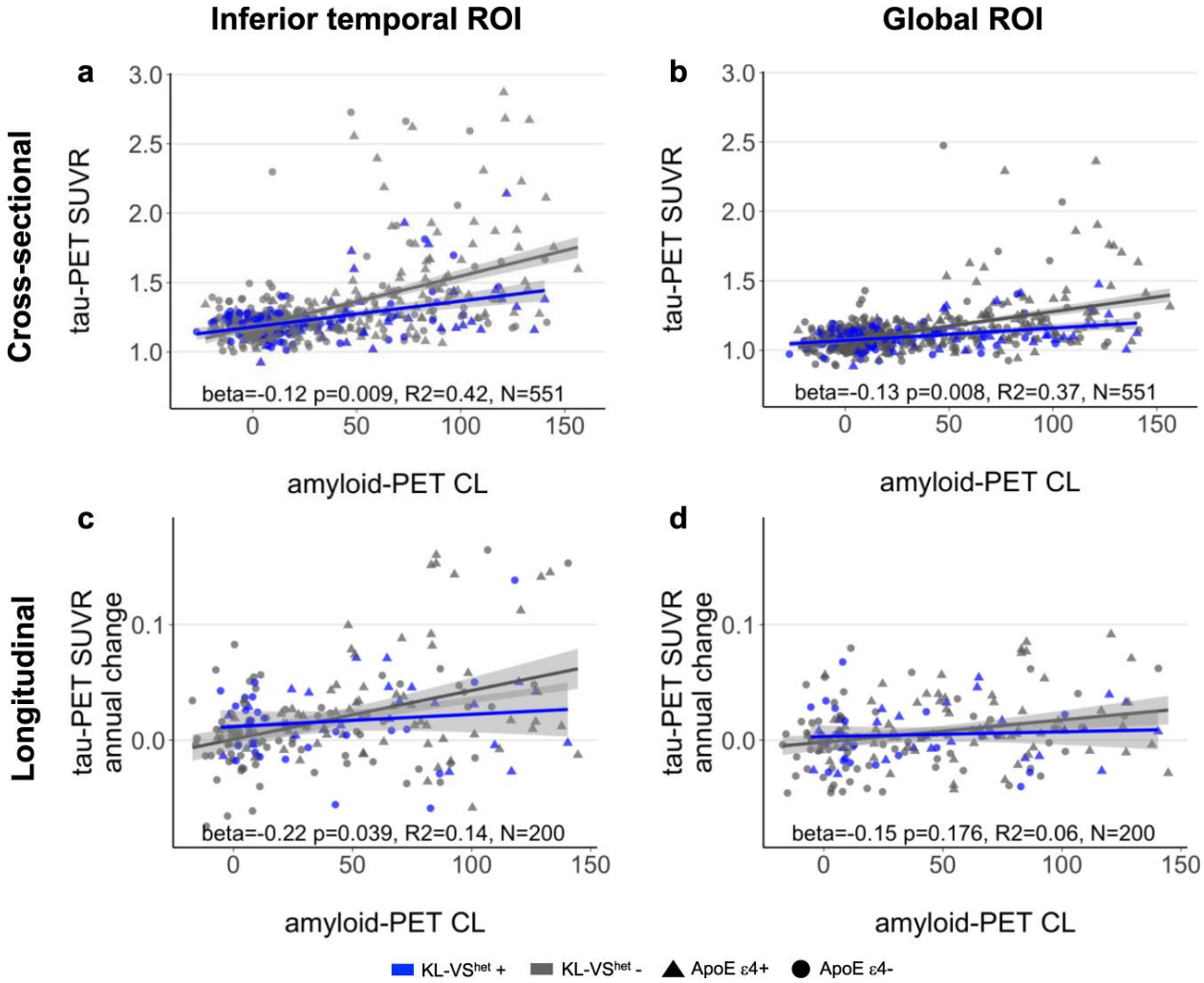

Figure S28. Association between KL-VS heterozygosity, amyloid-, and tau-PET. The relationship between global amyloid-PET levels and (A,B) cross-sectionally assessed tau-PET levels or (C,D) longitudinally assessed tau-PET annual change rates measured in inferior temporal gyri (left panel) and globally in neocortical areas (right panel) as a function of KL-VS^{het} variant. Blue and gray colors indicate individuals with heterozygous or non-heterozygous KL-VS alleles. Linear model fits are indicated together with 95% confidence intervals. Abbreviations: CL, centiloids; PET, positron emission tomography; ROI, region of interest; SUVR, standardized uptake value ratio. Reproduced under open access from [28].

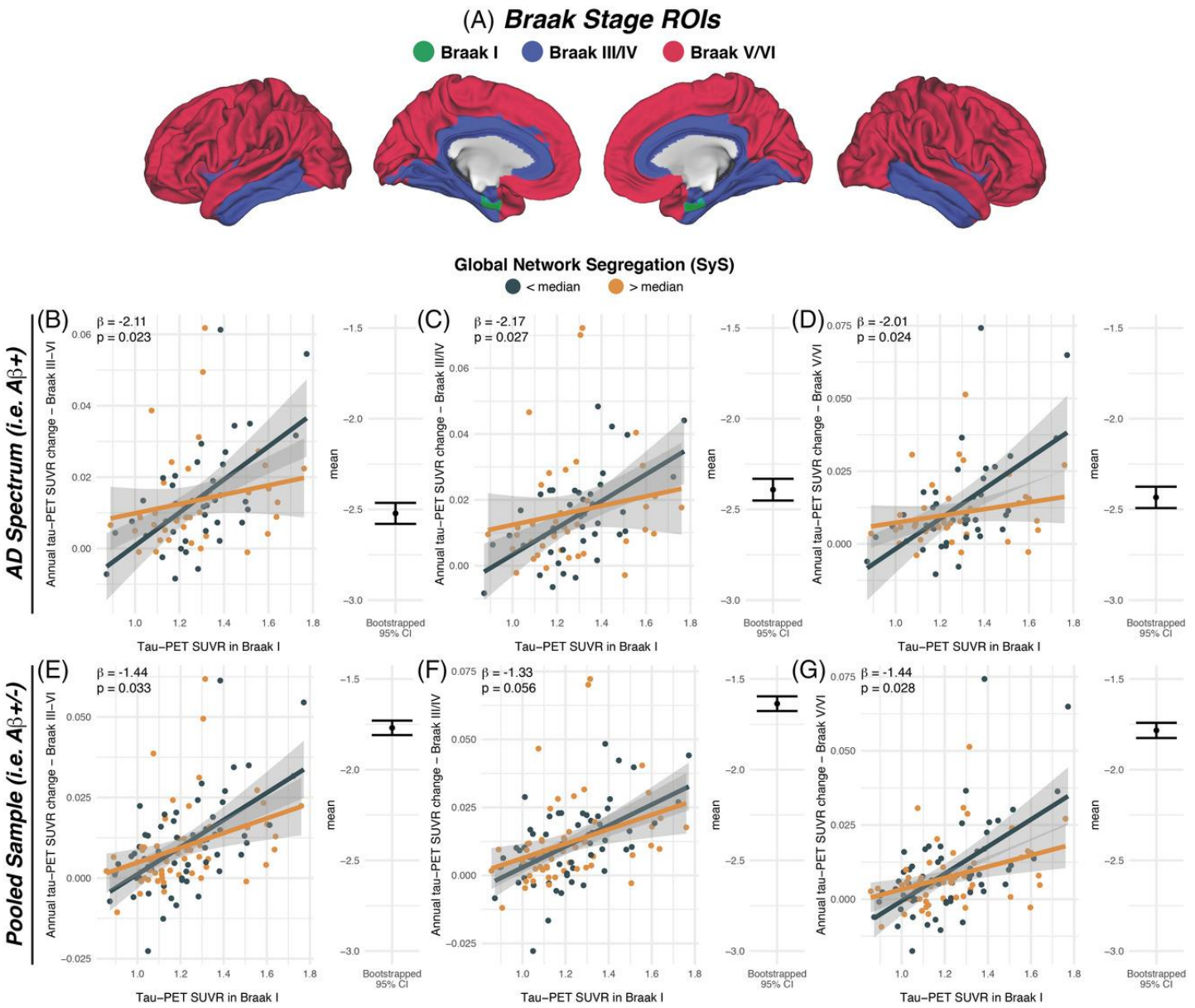

Figure S29. Association of functional network segregation with rate of tau accumulation in Braak stage regions. (A) Surface rendering of the Braak-staging regions of interest (ROIs) that were applied to tau positron emission tomography (PET) data to determine baseline tau PET levels and longitudinal tau PET changes. (B) Scatterplots illustrating the interaction effect between global network segregation (SyS) and entorhinal tau PET levels at baseline on tau PET increase in the remaining brain for amyloid beta positivity (Aβ+), showing that higher network segregation is associated with an attenuated association between entorhinal tau PET and tau accumulation in the rest of the brain. Exploratory analyses were performed in Aβ+ subjects, testing the same regression models for (C) earlier Braak regions III/IV and (D) late Braak regions V/VI. Analyses were repeated also including the Aβ− control group (E–G). 95% confidence intervals of interaction effects are displayed next to each scatterplot. SUVR, standardized uptake value ratio. Reproduced under open access from [29].

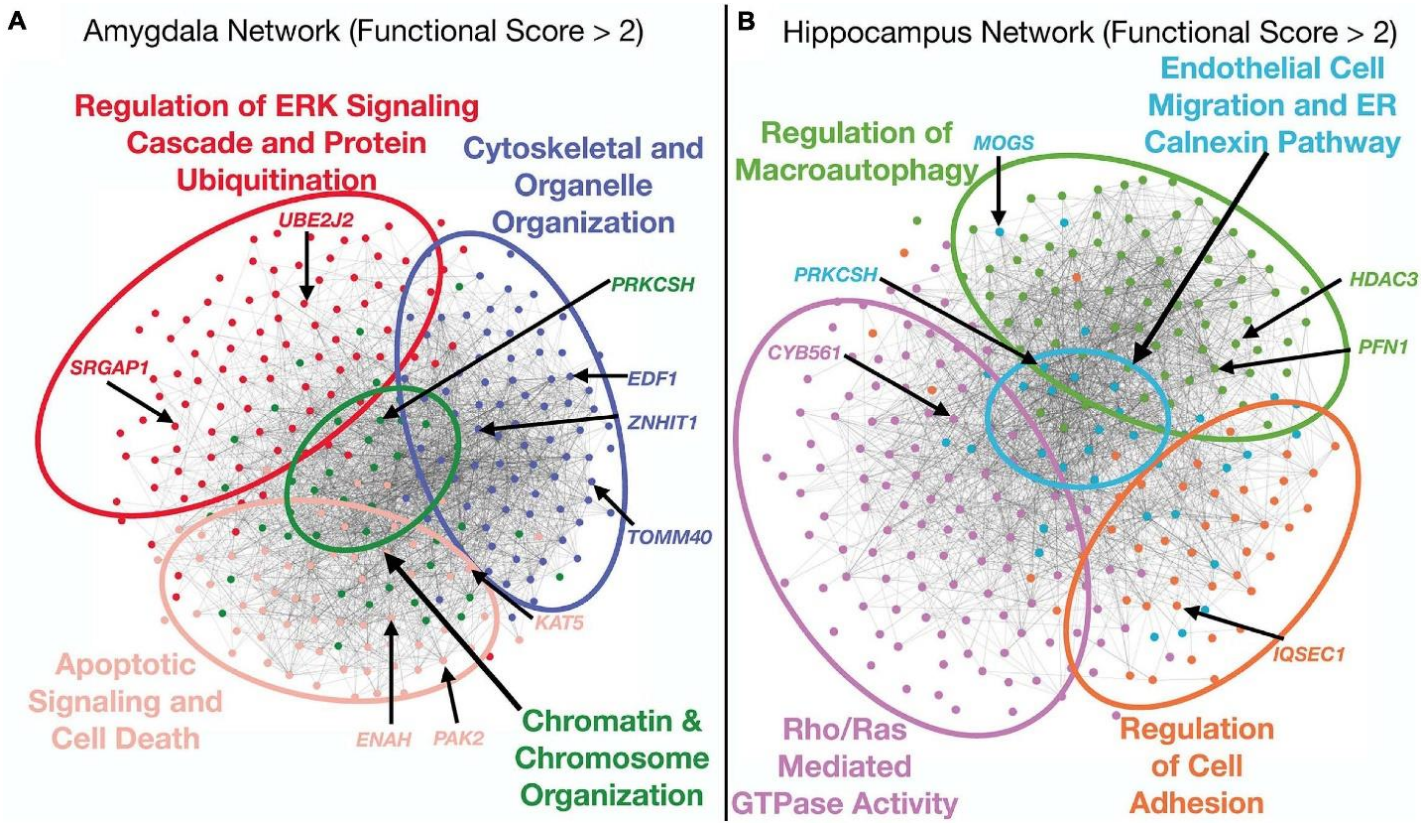

Figure S30. Analysis of top functional subnetworks identified in a GWAS of hippocampal and amygdala atrophy. (A) Amygdala sub-network analysis. The top functional sub-network for this tissue was enriched for genes in pathways that regulate apoptosis and cell death, cytoskeletal and organelle organization and chromosomal organization. (B) Hippocampus sub-network analysis. This top functional sub-network was enriched for genes involved in immune signaling as well as cell adhesion and ER regulation. Abbreviations: GWAS, genome wide association study. Reproduced under open access from [30].

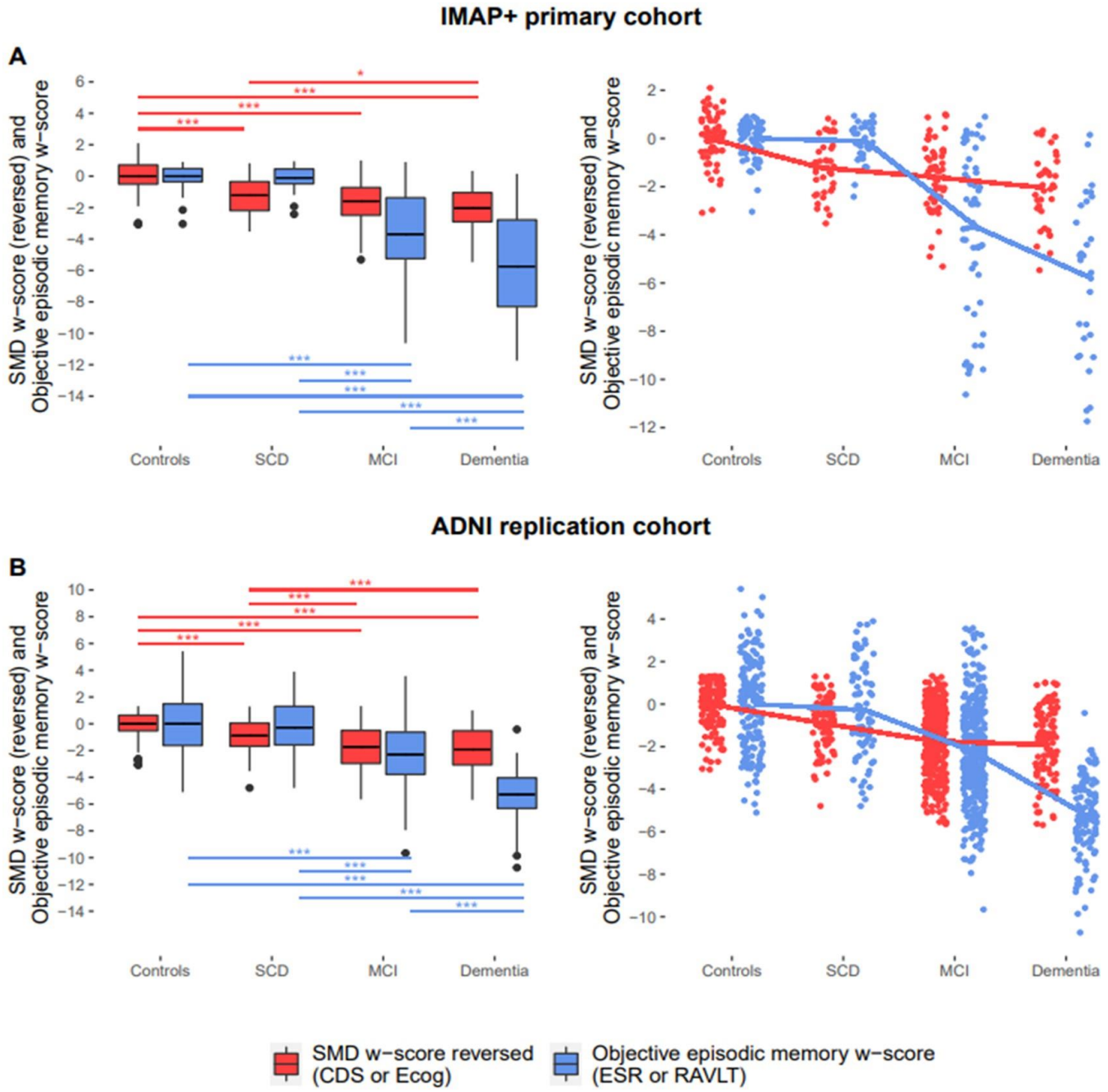

Figure S31. Between-group comparisons of the mean subjective and objective episodic memory scores within the two independent cohorts. Scores correspond to reversed subjective memory decline (SMD) ***w***-scores (in red) and objective episodic memory ***w***-scores (in blue), such that lower scores indicate greater subjective memory decline and poorer memory performances, respectively**. (**Left panel) Boxplot illustrating the results of *post hoc* Tukey-test after ANOVA showing the mean (bold horizontal line), interquartile range (box), total range (whiskers) and outliers (black dots). **(**Right panel**)** Graphs indicating the distribution of participants' values and average for each clinical group connected by a line. **(**A**)** Data for the IMAP+ primary cohort, with the CDS in red and the ESR in blue. (**B**) Data from the ADNI replication cohort, with the Ecog in red and the RAVLT in blue. **P* < 0.05, ***P* < 0.01, ****P* < 0.001 for the between-group comparisons. Abbreviations: CDS, Cognitive Difficulties Scale; Ecog, Everyday Cognition; ESR, encoding, storage, and retrieval; IMAP, Imagerie Mulitmodale de la maladie de Alzheimer a un stade Precoce; MCI, mild cognitive impairment; RAVLT, Rey Auditory Verbal Learning Test; SCD, subtle cognitive decline; Reproduced under open access from [31].

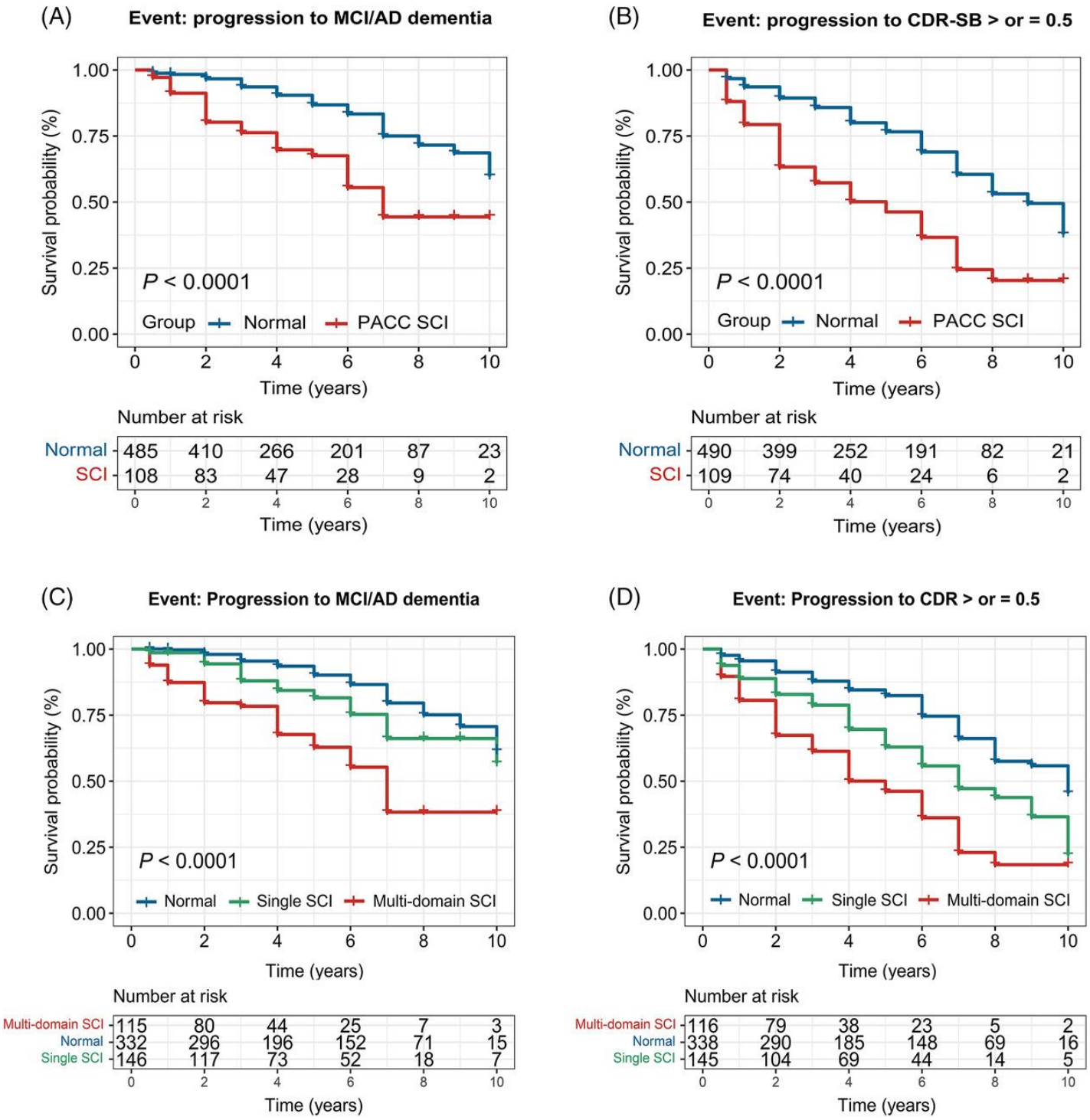

Figure S32. Survival probability of clinical progression in participants with subtle cognitive impairment. Kaplan-Meier curves showing survival probability of clinical progression. (A) and (C) Progression from cognitively normal participants to mild cognitive impairment or AD dementia. (B) and (D) Progression from cognitively normal participants to incident prodromal stage of AD indicated by a CDR-global score of 0.5 or greater. Stratification by presence or absence of subtle cognitive impairment is shown in (A) and (B), and by single and multi-domain subtle cognitive impairment in (C) and (D). Abbreviations: AD, Alzheimer's disease; CDR-SB, clinical dementia rating sum of boxes; MCI, mild cognitive impairment; PACC, pre-Alzheimer's cognitive composite; SCI, subtle cognitive impairment. Reproduced under open access from [32].

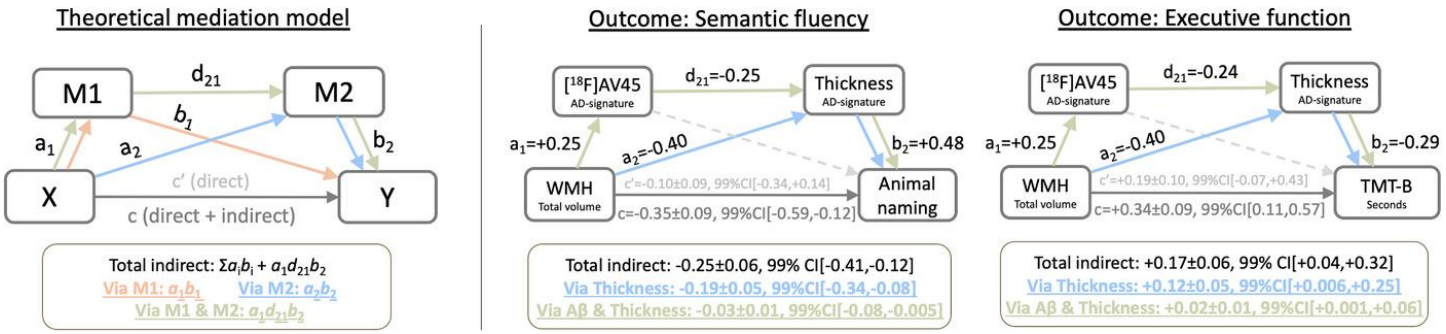

Figure S33. Mediation analyses of Aβ and atrophy on the white matter hyperintensity–cognition relationship. Left: Theoretical serial mediation model indicating the independent variable (X), dependent variable (Y), and two mediators (M1, M2). Middle/right: Aβ SUVR and atrophy are mediating the association of total WMH volumes with semantic fluency (middle) and executive function (right). Thick lines are part of a significant pathway, whereas dashed lines represent non-significant pathways. All mediators used an AD signature meta-ROI. Values are indicated as mean ± SE and 99% CI are bootstrapped with 5000 replications. Path c represents the total (direct + indirect) effect adjusted only for covariates (age, sex, education), whereas c' represents the direct effect adjusted for covariates and indirect effects. Abbreviations: Aβ, amyloid beta; AD, Alzheimer's disease; CI, confidence interval; ROI, region of interest; SE, standard error; SUVR, standardized uptake value ratio; TMT-B, Trail Making Test part-B; WMH, white matter hyperintensity. Reproduced under open access from (Ottoy et al 2022).

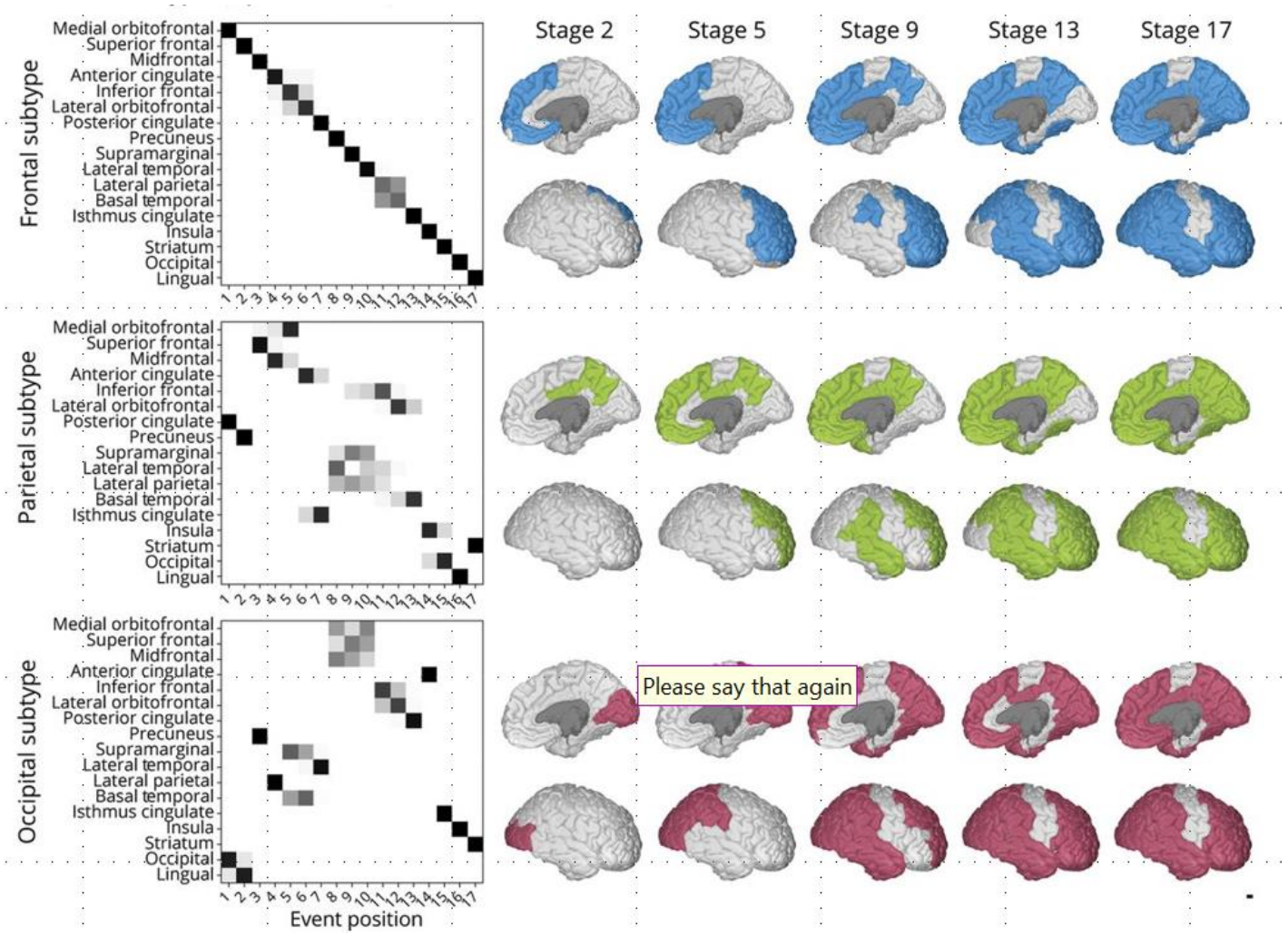

Figure S34. Representation of three amyloid β-based subtypes. Representation of the final 3 subtypes as identified by Subtype and Stage Inference (SuStaIn), referred to as frontal (top row), parietal (middle row), and occipital (bottom row), in accordance with the earliest regions to become abnormal. Reproduced under open access from [33].

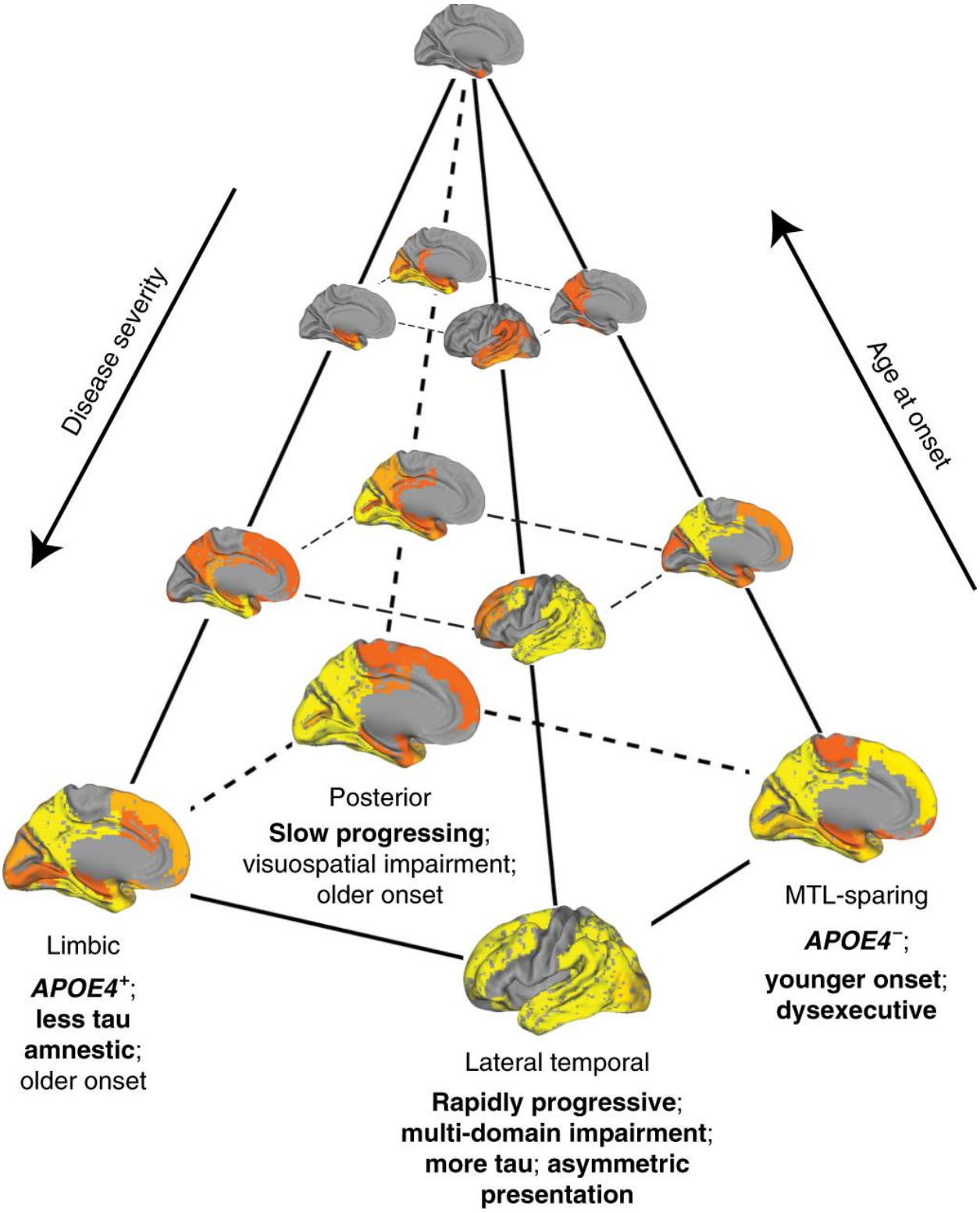

Figure S35. A theoretical model summarizing variation in the spread of tau pathology in AD. Tau pathology varies along an axis of severity (vertical in the diagram), which is inversely associated with age at onset. Four subtypes (limbic, medial temporal lobe (MTL) -sparing, lateral temporal, and posterior) are indicated. Reproduced from[34].

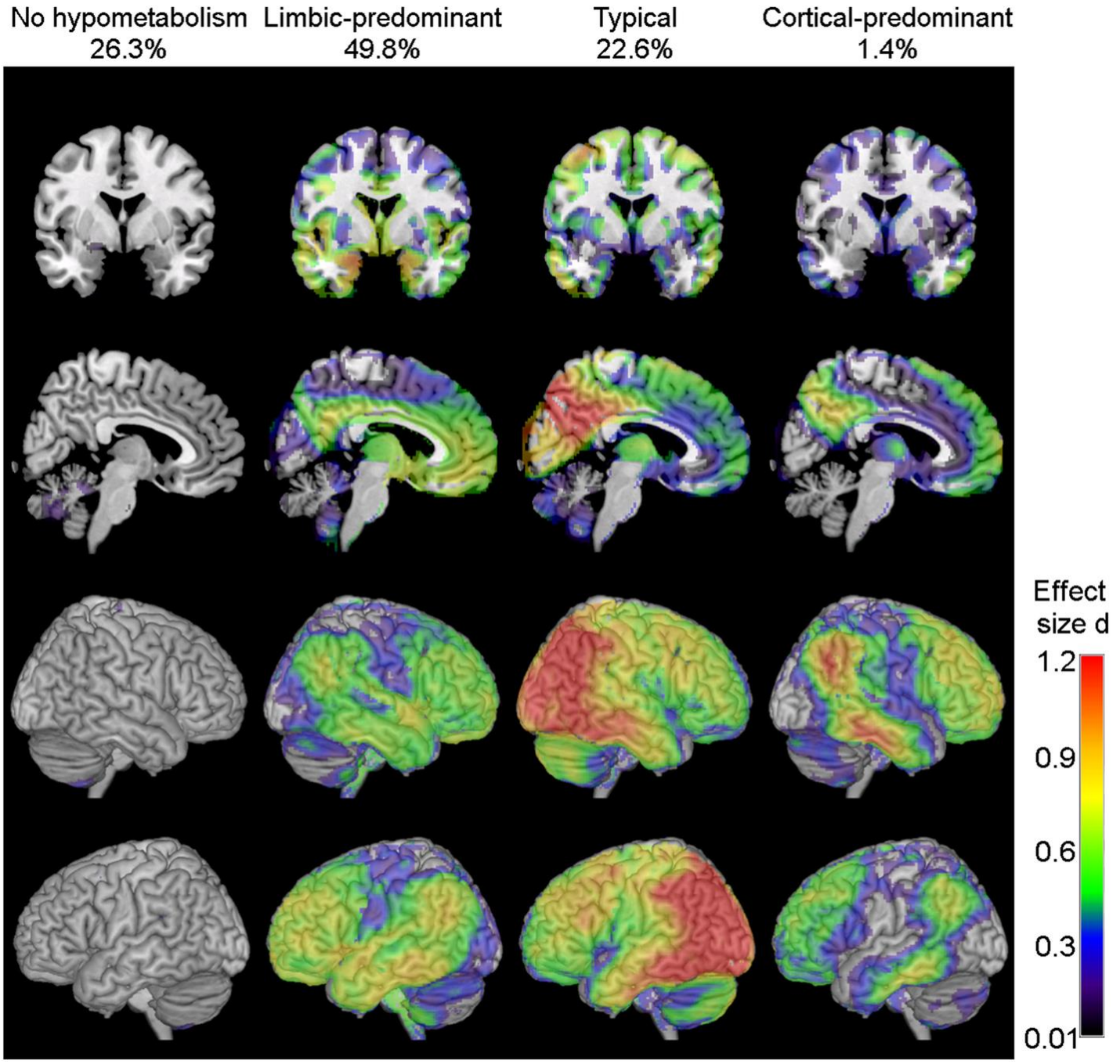

Figure S36. Data-driven FDG-PET subtypes of Alzheimer's disease-related neurodegeneration. Hypometabolic FDG-PET patterns of subtypes of patients with prodromal AD. Voxel-wise hypometabolic patterns of the four prodromal AD subtypes as compared to the healthy control group. Abbreviations: AD, Alzheimer's disease; FDG-PET, ^{18}F-fluorodeoxyglucose positron emission tomography. Reproduced under open access from[35].

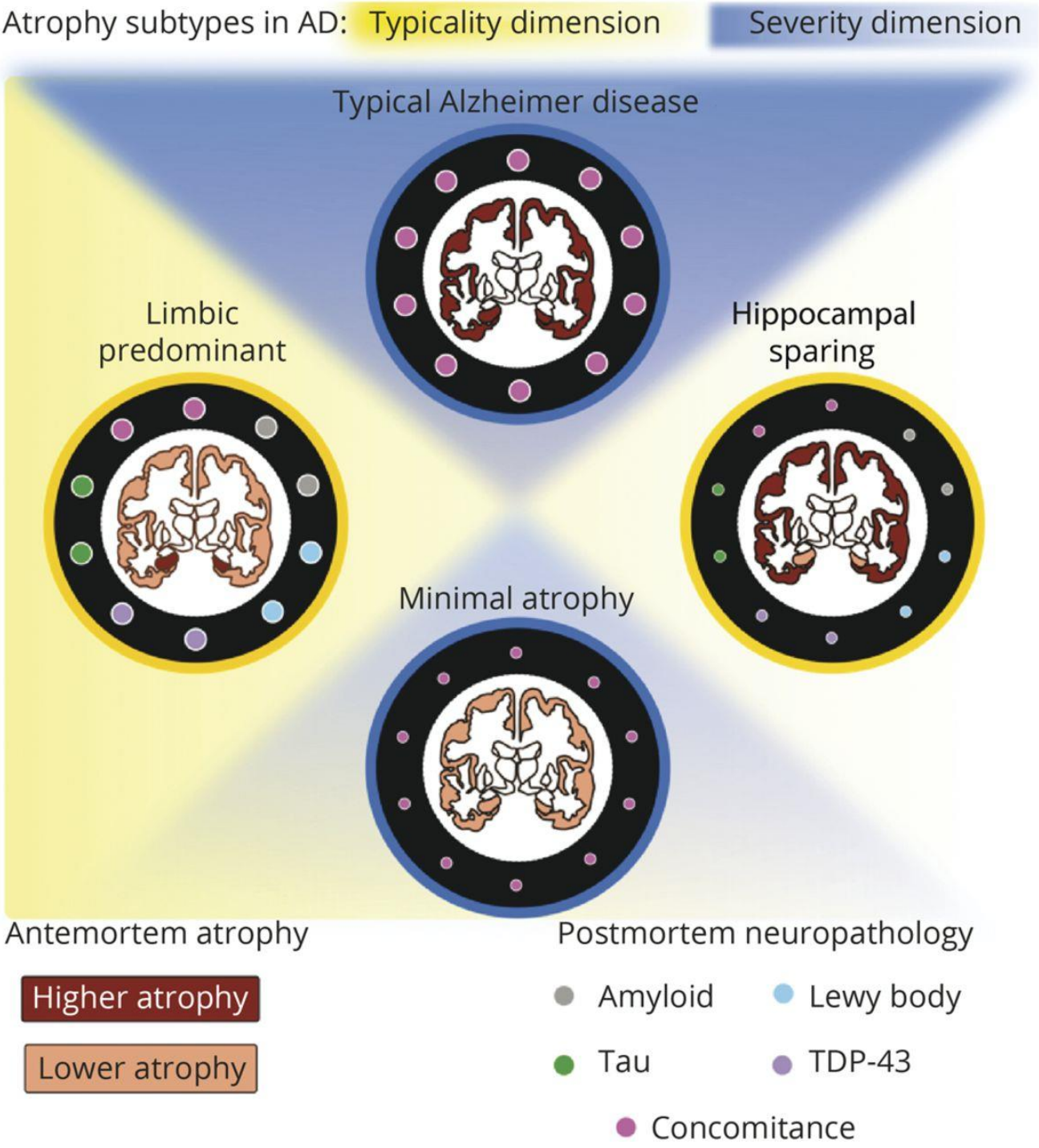

Figure S37. Susceptibility of antemortem MRI-based heterogeneity to AD and non-AD neuropathologies. Associations of antemortem typicality and severity with postmortem neuropathologic features may generate the following hypotheses: (1) the orthogonal dimensions of biological heterogeneity, typicality and severity, may offer complementary information regarding the vulnerability of the brain to AD (amyloid, tau) and non-AD (α-syn, TDP-43) pathologies; and (2) limbic-predominant AD along the typicality dimension and typical AD along the severity dimension may share similar underlying biological pathway(s), which make them more susceptible to pathologies, whereas hippocampal-sparing AD along the typicality dimension and minimal AD along the severity dimension may share similar pathway(s), making them less susceptible. Abbreviations: α-syn, α-synuclein; AD, Alzheimer disease; TDP-43, TAR DNA-binding protein 43. Reproduced under open access from [36].

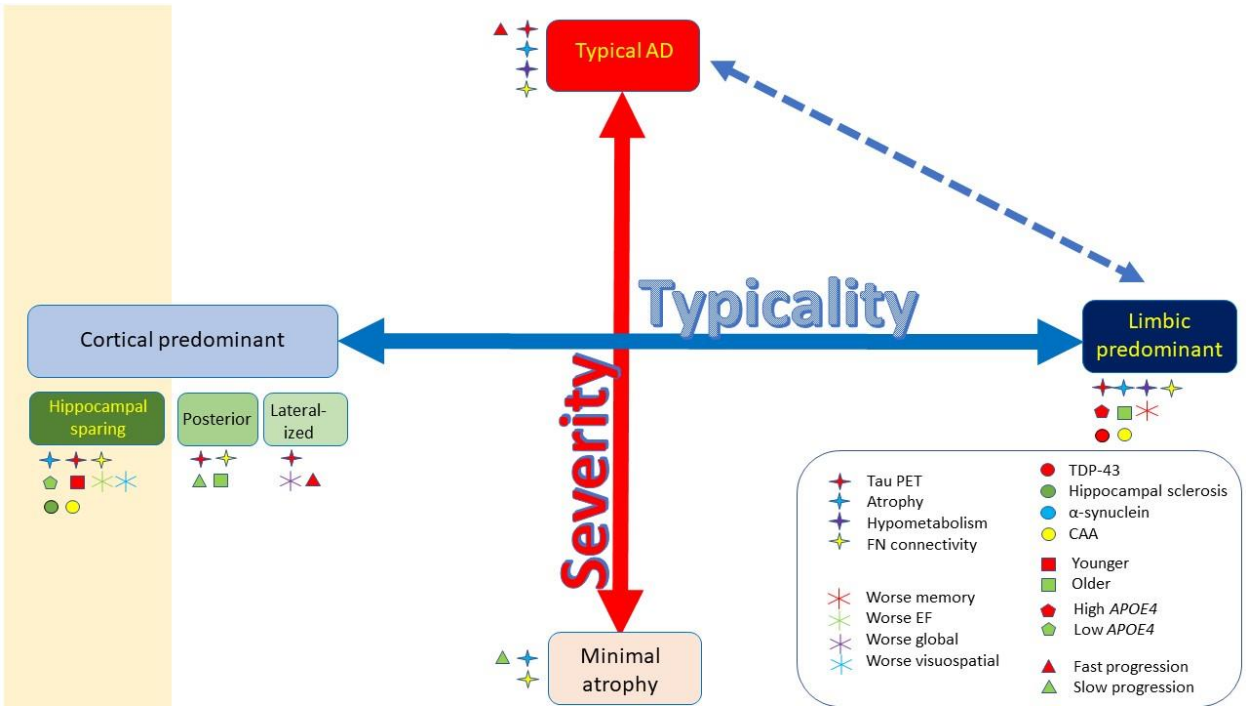

Figure S38. Schematic of biological subtypes determined by recent ADNI papers. According to the framework proposed by Ferreira et al. [37], atrophy subtypes exist on orthogonal axes of typicality, ranging from limbic predominant to cortical predominant, and severity, ranging from minimal atrophy to typical AD. Recent ADNI studies identified biological subtypes based on cortical tau deposition [34, 38-40] and neurodegeneration (atrophy [41, 42] and hypometabolism[35, 43, 44]). The subtypes show a degree of overlap, predominantly in the MTL [39], and are represented on the same framework. Modalities used for subtyping and defining characteristics (age, cognitive impairments, *APOE ε4* frequency, co-pathologies, rate of progression) are indicated. The limbic predominant subtype is most prevalent typicality subtype. A hippocampal sparing subtype was identified by multiple modalities and may represent a separate biological pathway, early onset AD, or AD with DLB (yellow section). Two cortical predominant subgroups were characterized by posterior and lateralized tau binding and atrophy and may represent atypical non-amnestic AD presentations such as posterior cortical atrophy and logopenic primary progressive aphasia, respectively. On the severity axis, the minimal atrophy subtype is characterized by slow progression and the least severe cognitive impairments. Typical AD is characterized by faster progression and more severe atrophy and cognitive impairments. The limbic predominant and typical AD subtypes showed concomitance with postmortem pathologies and are thought to be related (dashed line). The limbic predominant subtype may represent an intermediate stage of decline. Abbreviations: CAA, cerebral amyloid angiopathy; DLB, Dementia with Lewy bodies; EF, executive function; FN, functional; PET, positron emission tomography; TDP-43, TAR DNA binding protein 43.

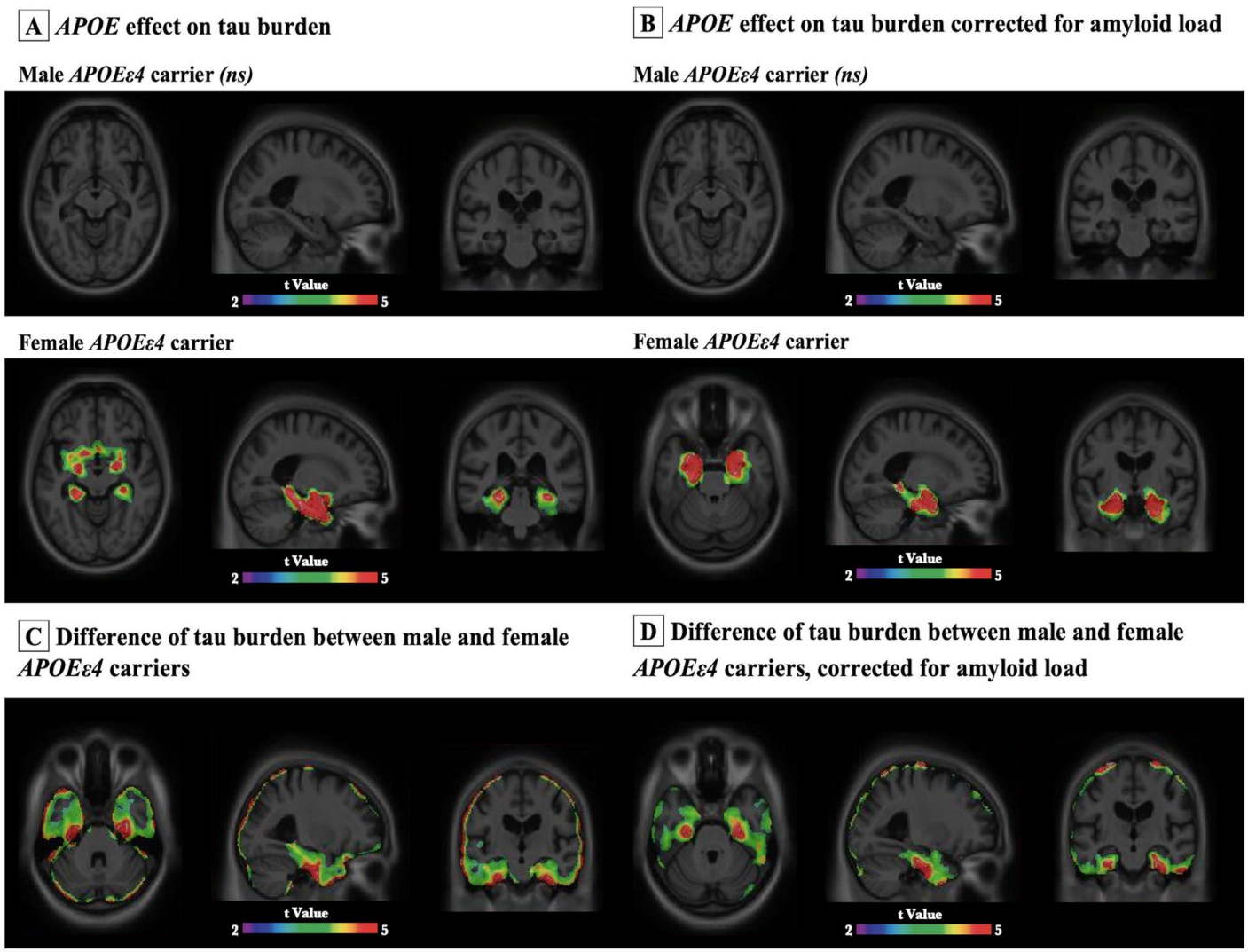

Figure S39. *APOE ε4* was associated with higher tau load in medial temporal regions in women but not in men. (A) No significant effect of *APOE* on tau burden was observed in males. Female *APOE ε4* carriers showed significantly higher [18F]MK6240 SUVRs in hippocampus, entorhinal and parahippocampal cortices as compared to female *APOE ε4* non-carriers. (B) After accounting for the amyloid load, there was no difference in tau burden between male *APOE ε4* carriers and non-carriers. Higher tau burden was found in female *APOE ε4* carriers versus noncarriers in hippocampus, entorhinal and parahippocampal cortices. (C and D) Female *APOE ε4* carriers showed significantly higher tau burden in medial temporal regions compared to male *APOE ε4* carriers (results remained significant after corrected for amyloid load). Abbreviations: ns, not significant. Reproduced under open access from[45].

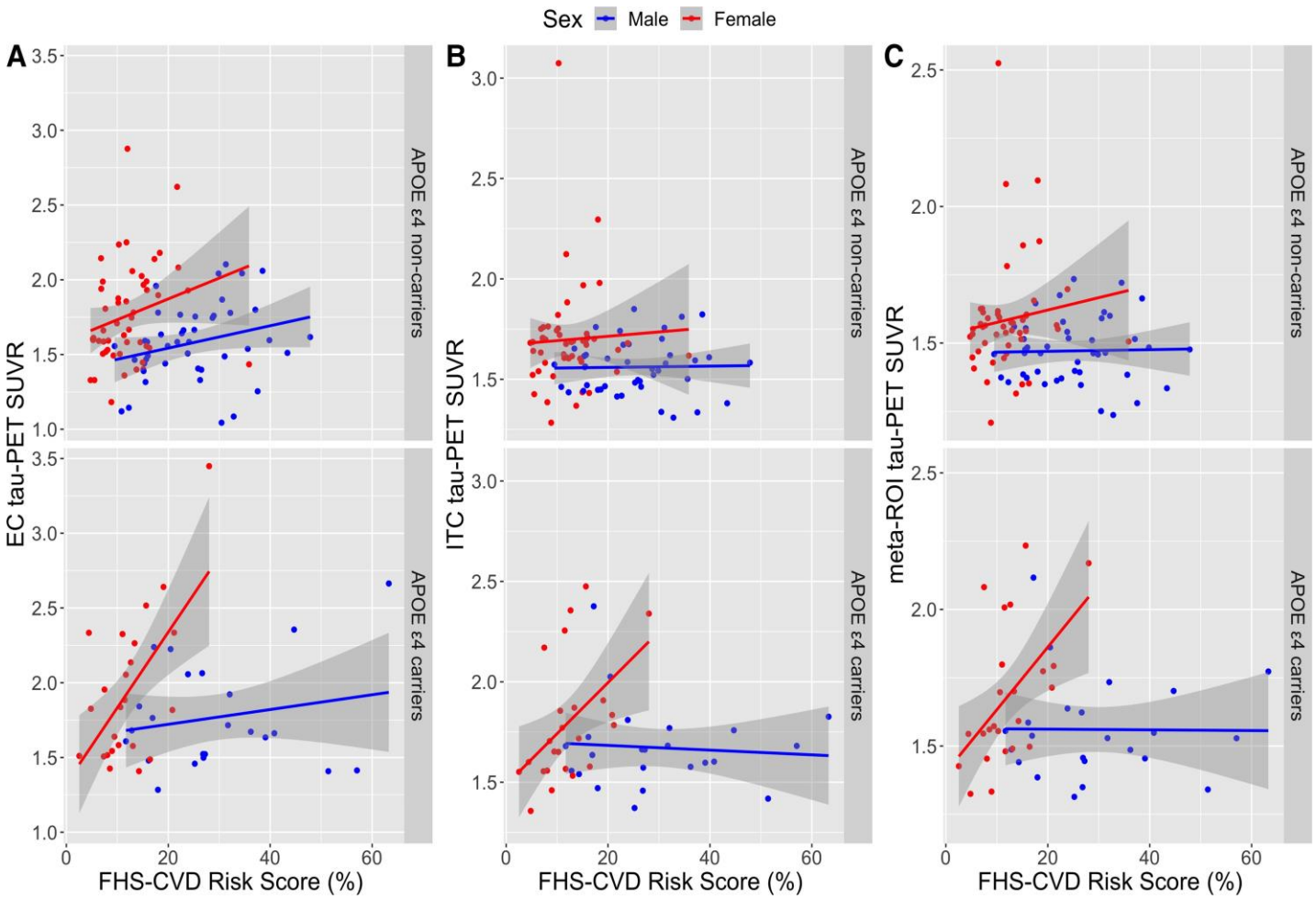

Figure S40. Sex and *APOE* ε4 modify associations between cardiovascular disease risk and tau deposition. Scatter plots depicting sex differences in associations between FHS-CVD risk score and tau deposition in the (A) entorhinal cortex, (B) inferior temporal cortex and (C) a composite temporal lobe meta-ROI, among *APOE ε4* non-carriers (top) and *APOE ε4* carriers (bottom). Shaded regions represent 95% confidence intervals. Significant interactions between sex and FHS-CVD risk on tau deposition were found in the EC (β = 0.05; 95% CI, 0.02–0.08; P = 0.001), ITC (β = 0.03; 95% CI, 0.01–0.05; P = 0.009) and meta-ROI (β = 0.02; 95% CI, 0.01–0.04; P = 0.008) among *APOE ε4* carriers (bottom) but not among non-carriers (top). Abbreviations: EC, entorhinal cortex; FHS-CVD, Framingham Heart Study Cardiovascular Disease risk score; ITC, inferior temporal cortex; ROI, region of interest. Reproduced under open access from[46].

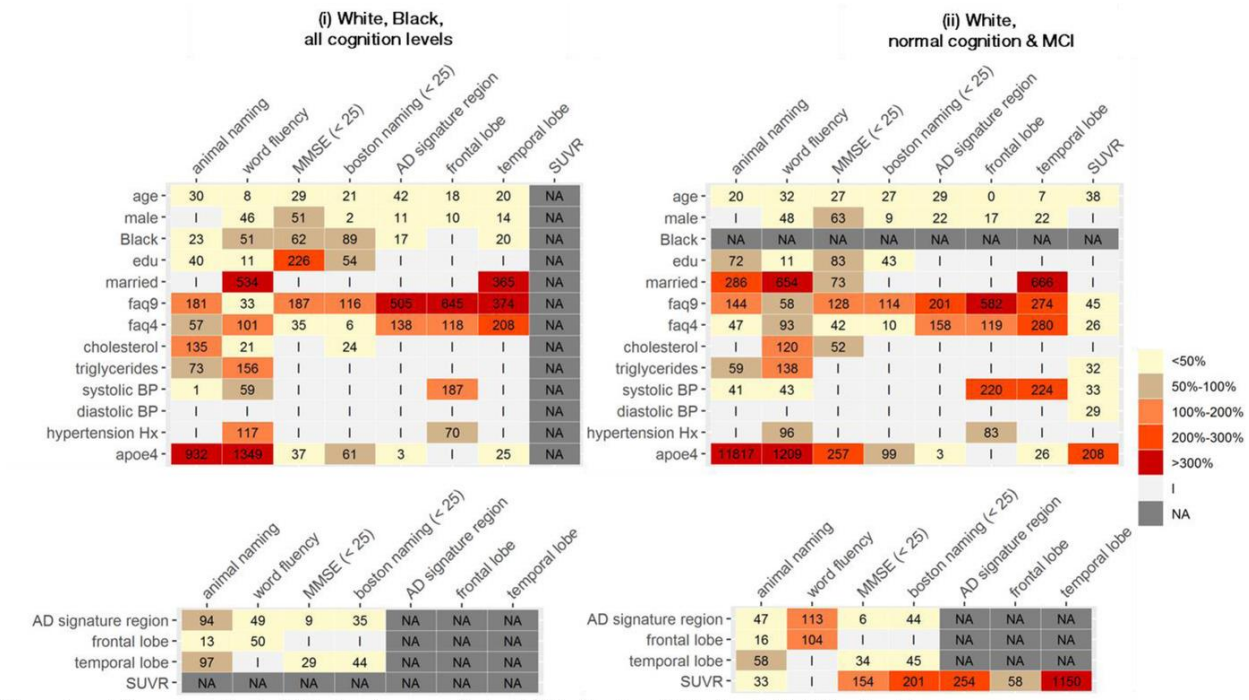

[a] Percentage difference relative to ARIC estimates, computed as |ARIC estimate – ADNI estimate|/|ARIC estimate|
NA: Association not applicable to sample
I: Association not significant to p<0.05 in either cohort

Figure S41. Differences in associations between risk factors and cognitive tests/imaging outcomes between ADNI and the Atherosclerosis Risk in Communities (ARIC) study. Heat map of percentage differences in point estimates of associations between risk factors and cognitive tests/imaging outcomes, and between imaging outcomes and cognitive test outcomes; limited to *P*<0.05 for at least one cohort. Abbreviations: AD, Alzheimer's disease; APOE, apolipoprotein E ε4 positive; BP, blood pressure; FAQ, Functional Activities Questionnaire; MMSE, Mini-Mental State Examination; SUVR, standardized uptake value ratio. Reproduced under open access from [47].

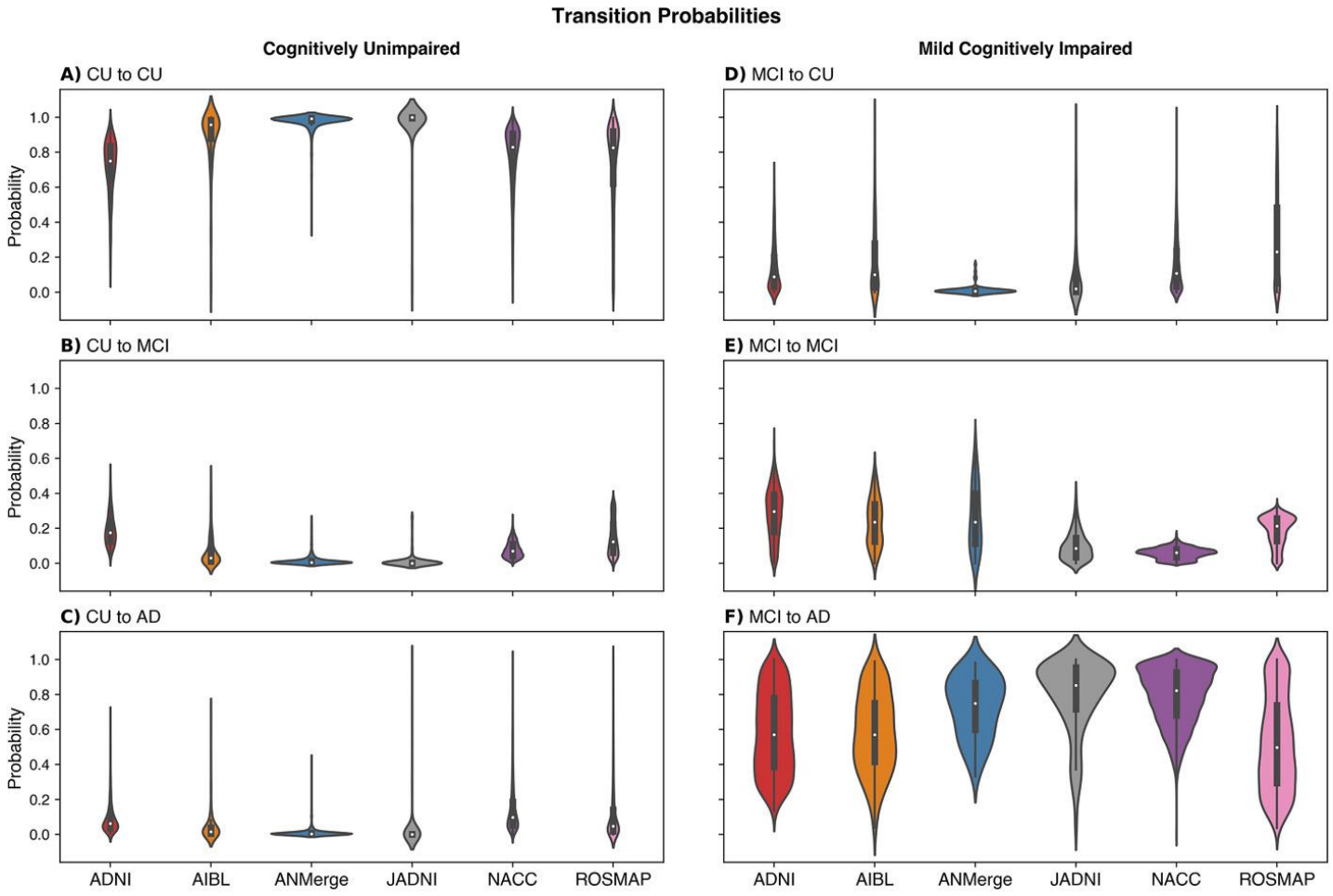

Figure S42. Probabilities of transition from one diagnostic state to another in six cohorts. Probabilities to transition from one state to another are estimated for a 10-year period. Median probabilities are marked with white points. Statistical distributions are shown as box plots as well as superimposed kernel density estimates, resulting in violin plots. (A-C) Transition probabilities starting from the cognitively unimpaired (CU) state. (D-F) Transition probabilities starting from the mild cognitive impairment (MCI) state. Abbreviations: AD, Alzheimer's disease; ADNI, Alzheimer's Disease Neuroimaging Initiative; AIBL, Australian Imaging, Biomarker & Lifestyle Flagship Study of Ageing; ANMerge, AddNeuroMed; J-ADNI, Japanese Alzheimer's Disease Neuroimaging Initiative; NACC, National Alzheimer's Coordinating Center; ROSMAP, Religious Orders Study and Rush Memory and Aging Project. Reproduced under open access from [48].

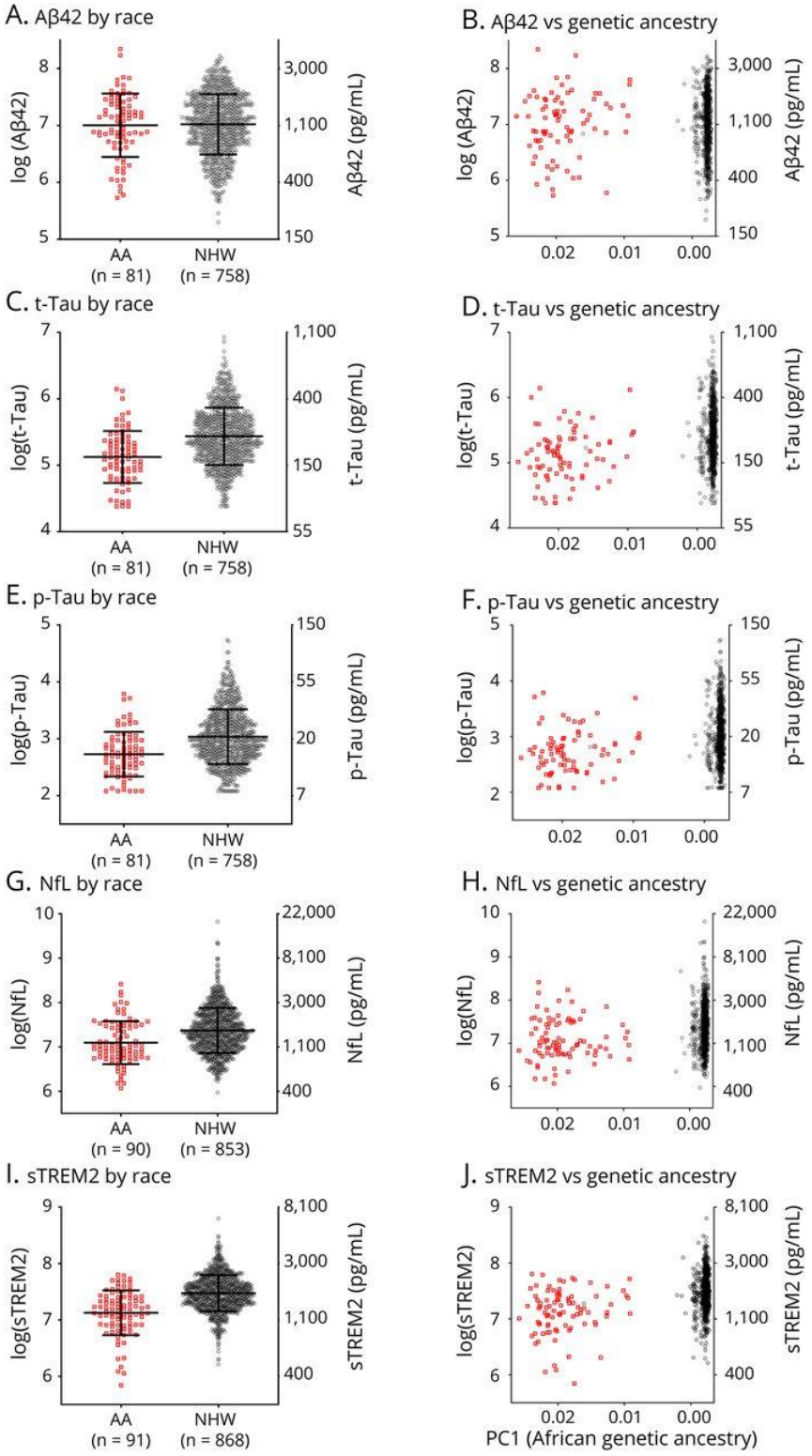

Figure S43. Differences in CSF biomarker concentrations by self-reported race. The natural logarithm of CSF concentrations of (A,B) Aβ42, (C,D) T-tau, (E,F) P-tau181, (G,H) NfL, and (I,J) sTREM2 as a function of self-reported race (African-American [AA] or non-Hispanic white (NHW) or a measure of African genetic ancestry (PC1, higher values correspond to higher African genetic ancestry, axis is reversed). Corresponding concentrations in pg/ml are shown on the right access. Red squares represent samples from AAs, and gray circles represent samples from NHW's. The number of individuals in each group is listed (n). Reproduced under open access from [49].

References

[1] Tahami Monfared AA, Tafazzoli A, Ye W, Chavan A, Zhang Q. Long-Term Health Outcomes of Lecanemab in Patients with Early Alzheimer's Disease Using Simulation Modeling. Neurology and therapy. 2022;11:863-80.
[2] Abi Nader C, Ayache N, Frisoni GB, Robert P, Lorenzi M, Alzheimer's Disease Neuroimaging I. Simulating the outcome of amyloid treatments in Alzheimer's disease from imaging and clinical data. Brain communications. 2021;3:fcab091.
[3] Salimi Y, Domingo-Fernández D, Bobis-Álvarez C, Hofmann-Apitius M, Birkenbihl C. ADataViewer: exploring semantically harmonized Alzheimer's disease cohort datasets. Alzheimer's research & therapy. 2022;14:69.
[4] Chen SD, Huang YY, Shen XN, Guo Y, Tan L, Dong Q, et al. Longitudinal plasma phosphorylated tau 181 tracks disease progression in Alzheimer's disease. Translational psychiatry. 2021;11:356.
[5] Bangen KJ, Thomas KR, Weigand AJ, Edmonds EC, Clark AL, Solders S, et al. Elevated plasma neurofilament light predicts a faster rate of cognitive decline over 5 years in participants with objectively-defined subtle cognitive decline and MCI. Alzheimer's & dementia : the journal of the Alzheimer's Association. 2021;17:1756-62.
[6] Moscoso A, Grothe MJ, Ashton NJ, Karikari TK, Lantero Rodriguez J, Snellman A, et al. Longitudinal Associations of Blood Phosphorylated Tau181 and Neurofilament Light Chain With Neurodegeneration in Alzheimer Disease. JAMA neurology. 2021;78:396-406.
[7] Ansart M, Epelbaum S, Bassignana G, Bone A, Bottani S, Cattai T, et al.

Predicting the progression of mild cognitive impairment using machine learning: A systematic, quantitative and critical review. Med Image Anal. 2021;67:101848.
[8] Hu WT, Ozturk T, Kollhoff A, Wharton W, Christina Howell J. Higher CSF sTNFR1-related proteins associate with better prognosis in very early Alzheimer's disease. Nature communications. 2021;12:4001.
[9] Biel D, Brendel M, Rubinski A, Buerger K, Janowitz D, Dichgans M, et al. Tau-PET and in vivo Braak-staging as prognostic markers of future cognitive decline in cognitively normal to demented individuals. Alzheimer's research & therapy. 2021;13:137.
[10] Ossenkoppele R, Reimand J, Smith R, Leuzy A, Strandberg O, Palmqvist S, et al. Tau PET correlates with different Alzheimer's disease-related features compared to CSF and plasma p-tau biomarkers. EMBO Mol Med. 2021;13:e14398.
[11] Therriault J, Vermeiren M, Servaes S, Tissot C, Ashton NJ, Benedet AL, et al. Association of Phosphorylated Tau Biomarkers With Amyloid Positron Emission Tomography vs Tau Positron Emission Tomography. JAMA Neurol. 2022.
[12] Bucci M, Chiotis K, Nordberg A, Alzheimer's Disease Neuroimaging I. Alzheimer's disease profiled by fluid and imaging markers: tau PET best predicts cognitive decline. Mol Psychiatry. 2021;26:5888-98.
[13] Vromen EM, de Boer SCM, Teunissen CE, Rozemuller A, Sieben A, Bjerke M, et al. Biomarker A+T-: is this Alzheimer's disease or not? A combined CSF and pathology study. Brain. 2022.
[14] Brum WS, de Bastiani MA, Bieger A, Therriault J, Ferrari-Souza JP, Benedet AL, et al. A three-range approach enhances the prognostic utility of CSF biomarkers in Alzheimer's disease. Alzheimers Dement (N Y). 2022;8:e12270.
[15] Iturria-Medina Y, Carbonell F, Assadi A, Adewale Q, Khan AF, Baumeister TR, et al. Integrating molecular, histopathological, neuroimaging and clinical neuroscience data with NeuroPM-box. Communications biology. 2021;4:20.
[16] Wang M, Sajobi TT, Ismail Z, Seitz D, Chekouo T, Forkert ND, et al. A pragmatic dementia risk score for patients with mild cognitive impairment in a memory clinic population: Development and validation of a dementia risk score using routinely collected data. Alzheimers Dement (N Y). 2022;8:e12301.
[17] Tosun D, Veitch D, Aisen P, Jack CR, Jr., Jagust WJ, Petersen RC, et al. Detection of β-amyloid positivity in Alzheimer's Disease Neuroimaging Initiative participants with demographics, cognition, MRI and plasma biomarkers. Brain communications. 2021;3:fcab008.
[18] Taylor A, Zhang F, Niu X, Heywood A, Stocks J, Feng G, et al. Investigating the temporal pattern of neuroimaging-based brain age estimation as a biomarker for Alzheimer's Disease related neurodegeneration. Neuroimage. 2022;263:119621.
[19] Adewale Q, Khan AF, Carbonell F, Iturria-Medina Y. Integrated transcriptomic and neuroimaging brain model decodes biological mechanisms in aging and Alzheimer's disease. eLife. 2021;10.
[20] Selkoe DJ, Hardy J. The amyloid hypothesis of Alzheimer's disease at 25 years. EMBO molecular medicine. 2016;8:595-608.
[21] Insel PS, Donohue MC, Berron D, Hansson O, Mattsson-Carlgren N. Time between milestone events in the Alzheimer's disease amyloid cascade. Neuroimage. 2021;227:117676.

[22] Kamagata K, Andica C, Takabayashi K, Saito Y, Taoka T, Nozaki H, et al. Association of MRI Indices of Glymphatic System With Amyloid Deposition and Cognition in Mild Cognitive Impairment and Alzheimer Disease. Neurology. 2022.
[23] Wang ZB, Ma YH, Sun Y, Tan L, Wang HF, Yu JT. Interleukin-3 is associated with sTREM2 and mediates the correlation between amyloid-β and tau pathology in Alzheimer's disease. J Neuroinflammation. 2022;19:316.
[24] Huang J, Tao Q, Ang TFA, Farrell J, Zhu C, Wang Y, et al. The impact of increasing levels of blood C-reactive protein on the inflammatory loci SPI1 and CD33 in Alzheimer's disease. Transl Psychiatry. 2022;12:523.
[25] Horgusluoglu E, Neff R, Song WM, Wang M, Wang Q, Arnold M, et al. Integrative metabolomics-genomics approach reveals key metabolic pathways and regulators of Alzheimer's disease. Alzheimer's & dementia : the journal of the Alzheimer's Association. 2022;18:1260-78.
[26] Nho K, Kueider-Paisley A, Arnold M, MahmoudianDehkordi S, Risacher SL, Louie G, et al. Serum metabolites associated with brain amyloid beta deposition, cognition and dementia progression. Brain communications. 2021;3:11.
[27] Franzmeier N, Ossenkoppele R, Brendel M, Rubinski A, Smith R, Kumar A, et al. The BIN1 rs744373 Alzheimer's disease risk SNP is associated with faster Abeta-associated tau accumulation and cognitive decline. Alzheimer's & dementia : the journal of the Alzheimer's Association. 2022;18:103-15.
[28] Neitzel J, Franzmeier N, Rubinski A, Dichgans M, Brendel M, Malik R, et al. KL-VS heterozygosity is associated with lower amyloid-dependent tau accumulation and memory impairment in Alzheimer's disease. Nature communications. 2021;12:3825.
[29] Steward A, Biel D, Brendel M, Dewenter A, Roemer S, Rubinski A, et al. Functional network segregation is associated with attenuated tau spreading in Alzheimer's disease. Alzheimer's & dementia : the journal of the Alzheimer's Association. 2022.
[30] Brabec JL, Lara MK, Tyler AL, Mahoney JM. System-Level Analysis of Alzheimer's Disease Prioritizes Candidate Genes for Neurodegeneration. Front Genet. 2021;12:625246.
[31] Kuhn E, Perrotin A, Tomadesso C, Andre C, Sherif S, Bejanin A, et al. Subjective cognitive decline: opposite links to neurodegeneration across the Alzheimer's continuum. Brain communications. 2021;3:15.
[32] Shen XN, Kuo K, Yang YX, Li HQ, Chen SD, Cui M, et al. Subtle cognitive impairment as a marker of Alzheimer's pathologies and clinical progression in cognitively normal individuals. Alzheimer's & dementia (Amsterdam, Netherlands). 2021;13:e12198.
[33] Collij LE, Salvado G, Wottschel V, Mastenbroek SE, Schoenmakers P, Heeman F, et al. Spatial-Temporal Patterns of beta-Amyloid Accumulation: A Subtype and Stage Inference Model Analysis. Neurology. 2022;98:e1692-e703.
[34] Vogel JW, Young AL, Oxtoby NP, Smith R, Ossenkoppele R, Strandberg OT, et al. Four distinct trajectories of tau deposition identified in Alzheimer's disease. Nature medicine. 2021;27:871-81.
[35] Levin F, Ferreira D, Lange C, Dyrba M, Westman E, Buchert R, et al. Data-driven FDG-PET subtypes of Alzheimer's disease-related neurodegeneration. Alzheimer's research & therapy. 2021;13:49.
[36] Mohanty R, Ferreira D, Frerich S, Muehlboeck JS, Grothe MJ, Westman E, et al. Neuropathologic Features of Antemortem Atrophy-Based Subtypes of Alzheimer Disease. Neurology. 2022.
[37] Ferreira D, Nordberg A, Westman E. Biological subtypes of Alzheimer disease: A systematic review and meta-analysis. Neurology. 2020;94:436-48.
[38] Frontzkowski L, Ewers M, Brendel M, Biel D, Ossenkoppele R, Hager P, et al. Earlier Alzheimer's disease onset is associated with tau pathology in brain hub regions and facilitated tau spreading. Nat Commun. 2022;13:4899.
[39] Toledo JB, Liu H, Grothe MJ, Rashid T, Launer L, Shaw LM, et al. Disentangling tau and brain atrophy cluster heterogeneity across the Alzheimer's disease continuum. Alzheimer's & dementia (New York, N Y). 2022;8:e12305.
[40] Young CB, Winer JR, Younes K, Cody KA, Betthauser TJ, Johnson SC, et al. Divergent Cortical Tau Positron Emission Tomography Patterns Among Patients With Preclinical Alzheimer Disease. JAMA Neurol. 2022;79:592-603.
[41] Mohanty R, Ferreira D, Frerich S, Muehlboeck JS, Grothe MJ, Westman E, et al. Neuropathologic Features of Antemortem Atrophy-Based Subtypes of Alzheimer Disease. Neurology. 2022;99:e323-33.
[42] Rauchmann BS, Ersoezlue E, Stoecklein S, Keeser D, Brosseron F, Buerger K, et al. Resting-State Network Alterations Differ between Alzheimer's Disease Atrophy Subtypes. Cereb Cortex. 2021;31:4901-15.
[43] Groot C, Risacher SL, Chen JQA, Dicks E, Saykin AJ, Mac Donald CL, et al. Differential trajectories of hypometabolism across cognitively-defined Alzheimer's disease subgroups. NeuroImage Clinical. 2021;31:102725.
[44] Tondo G, Carli G, Santangelo R, Mattoli MV, Presotto L, Filippi M, et al. Biomarker-based stability in limbic-predominant amnestic mild cognitive impairment. Eur J Neurol. 2021;28:1123-33.

[45] Wang YTT, Pascoal TA, Therriault J, Kang MS, Benedet AL, Savard M, et al. Interactive rather than independent effect of APOE and sex potentiates tau deposition in women. Brain communications. 2021;3:15.
[46] Tsiknia AA, Reas E, Bangen KJ, Sundermann EE, McEvoy L, Brewer JB, et al. Sex and APOE ε4 modify the effect of cardiovascular risk on tau in cognitively normal older adults. Brain communications. 2022;4:fcac035.
[47] Gianattasio KZ, Bennett EE, Wei J, Mehrotra ML, Mosley T, Gottesman RF, et al. Generalizability of findings from a clinical sample to a community-based sample: A comparison of ADNI and ARIC. Alzheimers Dement. 2021;17:1265 – 76.
[48] Birkenbihl C, Salimi Y, Frohlich H, Japanese Alzheimer's Dis N, Alzheimer's Dis N. Unraveling the heterogeneity in Alzheimer's disease progression across multiple cohorts and the implications for data-driven disease modeling. Alzheimers & Dementia. 2022;18:251-61.
[49] Schindler SE, Cruchaga C, Joseph A, McCue L, Farias FHG, Wilkins CH, et al. African Americans Have Differences in CSF Soluble TREM2 and Associated Genetic Variants. Neurol-Genet. 2021;7:12.